NATIONAL TECHNICAL UNIVERSITY OF ATHENS

SCHOOL OF CIVIL ENGINEERING

DEPARTMENT OF WATER RESOURCES AND ENVIRONMENTAL ENGINEERING

DIPLOMA THESIS:

Design optimization of hybrid renewable energy systems under uncertainty – The case of Sifnos island

ZISOS ATHANASIOS

Supervisor: Andreas Efstratiadis, Assistant Professor, NTUA

Table of Contents

Πρόλογος

Η παρούσα διπλωματική εργασία σηματοδοτεί το τέλος της φοίτησής μου στη Σχολή Πολιτικών Μηχανικών του Εθνικού Μετσοβίου Πολυτεχνείου. Πρόκειται για την απόρροια της συνεισφοράς όλων των ατόμων που αποτέλεσαν μέρος της ακαδημαϊκής μου εξέλιξης και αντικατοπτρίζει το πάθος και τον ζήλο που τρέφω για το παρόν αντικείμενο. Σε αυτή τη σελίδα θα ήθελα να εκφράσω την ευγνωμοσύνη μου προς τα άτομα αυτά.

Αρχικά, θα ήθελα να ευχαριστήσω θερμά τον κ. Ανδρέα Ευστρατιάδη, επίκουρο καθηγητή Ε.Μ.Π, για την επίβλεψη της διπλωματικής μου εργασίας. Η συμβολή του στην επιλογή ενός επίκαιρου θέματος που εκπροσωπεί τα επιστημονικά μου ενδιαφέροντα, καθώς και οι εποικοδομητικές του παρατηρήσεις υπήρξαν καθοριστικοί παράγοντες για την ομαλή υλοποίηση και συγγραφή της εργασίας αυτής.

Στην συνέχεια θα ήθελα να ευχαριστήσω ολόκαρδα την Υποψήφια Δρ. Τζωρτζίνα Σακκή. Οι αδιάκοπες παρεμβάσεις της και η προθυμία της να μοιραστεί τις γνώσεις της συνέβαλαν σε μεγάλο βαθμό στην τελική μορφή που έλαβε η εργασία. Η συνεισφορά της αυτή θα έχει πάντα μια ιδιαίτερη θέση στην ακαδημαϊκή μου σταδιοδρομία.

Ένα μεγάλο ευχαριστώ οφείλω επίσης και στον Δρ. Ιωάννη Τσουκαλά, για την κρίσιμη του συνεισφορά στην παροχή απαραίτητων δεδομένων για την διεκπεραίωση της εργασίας.

Τέλος, θα ήθελα να ευχαριστήσω τους γονείς μου, διότι χωρίς την συνεχή τους στήριξη και ενθάρρυνση δεν θα μπορούσα να επιτύχω τους στόχους που έχω θέσει, αλλά και τους φίλους μου που υπήρξαν συνοδοιπόροι μου σε αυτό το ταξίδι.

Ζήσος Αθανάσιος

Αθήνα, Μάρτιος 2023

Abstract

The European Green deal has set the goal of increasing renewable energy penetration in European countries' power systems, in an attempt to also reduce their carbon footprint. With regard to this, hybrid systems, combining renewables with energy storage components, have become increasingly popular. Their versatility allows for the exploitation of the complementary features of different energy sources. Hybrid energy systems find great applicability in remote regions that are typically not connected to the mainland power grid, where the energy independence challenge intensifies. In this thesis, we consider the optimization of a proposed scheme in the Greek island of Sifnos, comprising wind turbines, solar panels, and a pumped storage system using seawater, which introduces additional technical challenges to address. The rational design for the main system components is based on two pillars. The first is a multi-criteria financial optimization procedure that accounts for investment costs, energy market revenues and reliability metrics. The second pillar is a novel representation of key uncertainty sources, including two external drivers, namely the wind velocity (natural process) and the energy demand (anthropogenic process), and the wind-to-power conversion (internal process). The latter originates from the deviation of on-site wind power production from the manufacturer's power curve. The outcomes of the overall stochastic optimization procedure are compared to the mainstream deterministic design approach. In this vein, we employ a comprehensive interpretation of the impacts of uncertainty in hybrid energy system planning.

Ελληνική Περίληψη

Η Ευρωπαϊκή Πράσινη Συμφωνία έθεσε ως στόχο την αύξηση διείσδυσης των ανανεώσιμων πηγών ενέργειας στο ενεργειακό μίγμα των Ευρωπαϊκών χωρών, σε μία προσπάθεια μείωσης του αποτυπώματος άνθρακα. Αναφορικά με αυτό, τα υβριδικά συστήματα, συνδυάζοντας ανανεώσιμες πηγές και μέσα αποθήκευσης ενέργειας έχουν γίνει ευρέως διαδεδομένα. Η ευελιξία τους επιτρέπει την αξιοποίηση των παροχών διαφόρων πηγών ενέργειας. Τα υβριδικά ενεργειακά συστήματα βρίσκουν ιδιαίτερη εφαρμοσιμότητα σε απόμερες περιοχές που δεν είναι συνδεδεμένες με το κεντρικό δίκτυο ηλεκτρισμού της χώρας, όπου η ανάγκη ενεργειακής αυτονομίας εντείνεται. Στην παρούσα διπλωματική εργασία, πραγματοποιούμε τη βελτιστοποίηση ενός προτεινόμενου σχεδίου στο νησί της Σίφνου που περιλαμβάνει ανεμογεννήτριες, φωτοβολταϊκά και ένα σύστημα αντλησοταμίευσης που χρησιμοποιεί θαλασσινό νερό, γεγονός το οποίο εντάσσει επιπλέον τεχνικές προκλήσεις. Ο ορθολογικός σχεδιασμός για τα επιμέρους κύρια εξαρτήματα του συστήματος βασίζεται σε δύο πυλώνες. Ο πρώτος είναι μια οικονομική βελτιστοποίηση πολλαπλών κριτηρίων που λαμβάνει υπόψιν το κόστος επένδυσης, τα έσοδα από την πώληση ενέργειας και την αξιοπιστία του συστήματος. Ο δεύτερος πυλώνας αποτελεί μια καινοτόμο αναπαράσταση της αβεβαιότητας μέσω δύο εξωτερικών πηγών, την ταχύτητα ανέμου (φυσική διεργασία), την ζήτηση ηλεκτρικής ενέργειας (ανθρωπογενής διεργασία) και την μετατροπή ανέμου σε ενέργεια (εσωτερική διεργασία). Η τελευταία πηγή αβεβαιότητας προκύπτει από την απόκλιση που παρατηρείται στην παραγωγή ενέργειας από μια ανεμογεννήτρια στο πεδίο σε σχέση με την θεωρητική καμπύλη των κατασκευαστών. Τα αποτελέσματα αυτής της στοχαστικής μεθόδου βελτιστοποίησης συγκρίνονται με την ντετερμινιστική μέθοδο σχεδιασμού. Σε αυτό το πλαίσιο, διερμηνεύουμε την επιρροή της αβεβαιότητας κατά τον σχεδιασμό υβριδικών ενεργειακών συστημάτων.

Εκτενής περίληψη

Αντικείμενο της παρούσας διπλωματικής εργασίας αποτελεί η βελτιστοποίηση υβριδικού ενεργειακού συστήματος υπό καθεστώς αβεβαιότητας. Συγκεκριμένα, πραγματοποιείται οικονομική βελτιστοποίηση ενός προτεινόμενου υβριδικού ενεργειακού συστήματος στη Σίφνο, το οποίο χρησιμοποιεί σύστημα αντλησοταμίευσης με θαλασσινό νερό, μέσω εξελικτικού αλγορίθμου στο προγραμματιστικό περιβάλλον Rstudio.

Τα τελευταία χρόνια, η συνεχής αύξηση των ενεργειακών αναγκών, σε συνδυασμό με τις μη ευνοϊκές συνθήκες εισαγωγών και εξαγωγών ενέργειας, έχουν στρέψει το ενδιαφέρον στις ανανεώσιμες πηγές ενέργειας (ΑΠΕ). Οι ΑΠΕ, ανεξάντλητες και φιλικές προς το περιβάλλον, αποτελούν τους πυλώνες για την επίτευξη των στόχων που τέθηκαν στην Συμφωνία του Παρισίου και αυτών της βιώσιμης ανάπτυξης (SDGs) που όρισε ο Οργανισμός Ηνωμένων Εθνών (ΟΗΕ) κατά της κλιματικής αλλαγής και της καθολικής πρόσβασης σε ενέργεια.

Η πρόκληση για καθολική πρόσβαση σε ενέργεια οξύνεται σε απόμερες περιοχές και σε περιοχές που δεν είναι συνδεδεμένες με το κύριο δίκτυο παραγωγής ενέργειας, όπως τα νησιά. Τα υβριδικά ενεργειακά συστήματα με μέσα αποθήκευσης ενέργειας μπορούν να προσφέρουν ενεργειακή αυτονομία στις περιοχές αυτές. Ωστόσο, για να επιτευχθούν υψηλά επίπεδα αξιοπιστίας στην κάλυψη των ενεργειακών αναγκών απαιτείται η προσθήκη διαφόρων πτυχών αβεβαιότητας κατά τον σχεδιασμό των συστημάτων αυτών.

Τα υβριδικά συστήματα συνδυάζουν διάφορες μορφές ΑΠΕ (ηλιακή, αιολική) για την κάλυψη των ενεργειακών αναγκών. Τα συστήματα αυτά συμπληρώνονται από μέσα αποθήκευσης ενέργειας που αξιοποιούνται κατά τις περιπτώσεις περίσσειας και ελλειμμάτων ενέργειας. Η αντλησοταμίευση αποτελεί ένα από τα πιο αξιόπιστα μέσα αποθήκευσης ενέργειας. Αποτελείται από δύο ταμιευτήρες που βρίσκονται σε υψομετρική διαφορά εκατοντάδων μέτρων. Κατά τις περιόδους περίσσειας ενέργειας, νερό αντλείται και αποθηκεύεται στον ανάντη ταμιευτήρα, ενώ κατά τις περιόδους ελλειμμάτων, αξιοποιείται το διαθέσιμο ύψος πτώσης και παράγεται υδροηλεκτρική ενέργεια μέσω στροβίλων. Η **Εικόνα 1** αποτελεί σχηματική απεικόνιση ενός υβριδικού συστήματος.

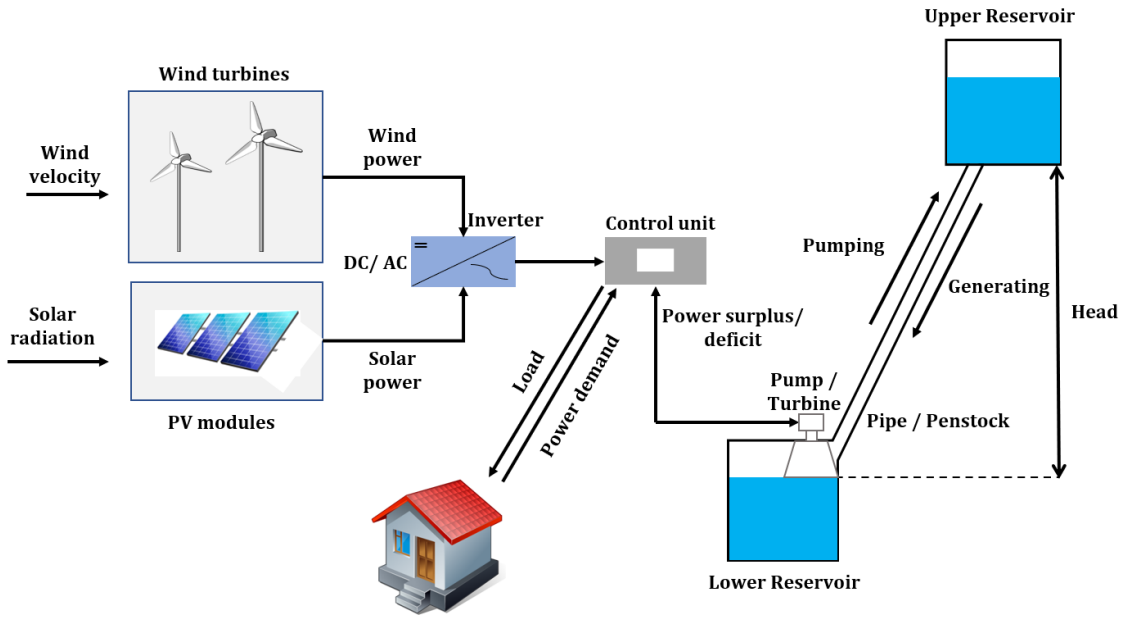

Εικόνα 1: Τυπική διάταξη υβριδικού ενεργειακού συστήματος με αντλησοταμίευση

Το υπό μελέτη υβριδικό σύστημα της Σίφνου είχε αρχικά προταθεί σε δημοσίευση των Δ. Κατσαπρακάκη και Μ. Βουμβουλάκη (2018). Πρόκειται για ένα υβριδικό σύστημα που συνδυάζει ηλιακή και αιολική ενέργεια με αντλησοταμίευση. Η ιδιαιτερότητα του συγκεκριμένου συστήματος οφείλεται στο γεγονός ότι η αντλησοταμίευση χρησιμοποιεί θαλασσινό νερό, θεωρώντας την θάλασσα ως τον κατάντη ταμιευτήρα. Το προαναφερόμενο σύστημα, αν και παρουσιάζει υψηλή αξιοπιστία, έχει δύο κύρια μειονεκτήματα: (1) δεν λαμβάνει υπόψιν το καθεστώς της αβεβαιότητας και (2) προτείνει ένα έργο μεγάλης κλίμακας που τόσο τεχνικά, όσο και οικονομικά, δεν είναι εφικτό να υλοποιηθεί.

Στην παρούσα διπλωματική εργασία προτείνουμε και βελτιστοποιούμε τον σχεδιασμό ενός υβριδικού έργου μικρότερης κλίμακας υπό καθεστώς αβεβαιότητας, διατηρώντας ταυτόχρονα το υψηλό επίπεδο αξιοπιστίας. Τα επιμέρους χαρακτηριστικά του προτεινόμενου υβριδικού συστήματος παρουσιάζονται στην **Εικόνα 2**. Η χρήση συστήματος αντλησοταμίευσης με θαλασσινό νερό παρουσιάζει τεχνικές προκλήσεις, ήτοι την διάβρωση του αγωγού πτώσης και του μηχανολογικού εξοπλισμού και τον κίνδυνο υφαλμύρωσης του υδροφορέα σε περίπτωση διαφυγών, στις οποίες προτείνονται τρόποι αντιμετώπισης.

Κατά τον σχεδιασμό λαμβάνονται υπόψιν διάφορες πτυχές της αβεβαιότητας. Όσον αφορά την εξωγενή αβεβαιότητα, παράγονται συνθετικές χρονοσειρές ταχυτήτων ανέμου και ζήτησης ηλεκτρικής ενέργειας. Οι χρονοσειρές αυτές παράγονται σε ωριαία βάση, έχουν μήκος 20 ετών και διατηρούν τα ίδια στατιστικά χαρακτηριστικά με τις ιστορικές χρονοσειρές. Από την άλλη, η ενδογενής αβεβαιότητα εκφράζεται μέσω της αβεβαιότητας που εντάσσεται στην καμπύλη παραγωγής ενέργειας των ανεμογεννητριών. Συγκεκριμένα, θεωρούμε πως, για κάθε ταχύτητα ανέμου, η παραγόμενη ενέργεια εκφράζεται από ένα πλήθος σημείων που ακολουθεί κανονική κατανομή, με συνολική μέση απόκλιση από την καμπύλη των κατασκευαστών της τάξης 15%. Τέλος, κατά την λειτουργία των ανεμογεννητριών, θεωρούμε πως υλοποιείται η στρατηγική “soft cut-out”, δηλαδή μόλις οι τιμές ταχύτητας ανέμου ξεπεράσουν το όρια ασφαλείας (25 m/s) και

μέχρι ένα όριο εύλογων τιμών (30 m/s), η ανεμογεννήτρια δεν σβήνει, αλλά εξακολουθεί να παράγει λιγότερη ενέργεια, αλλάζοντας την γωνία κλίσης των πτερωτών. Η **Εικόνα 3** παρουσιάζει ένα παράδειγμα προτεινόμενης προσομοιωμένης καμπύλης ανεμογεννήτριας.

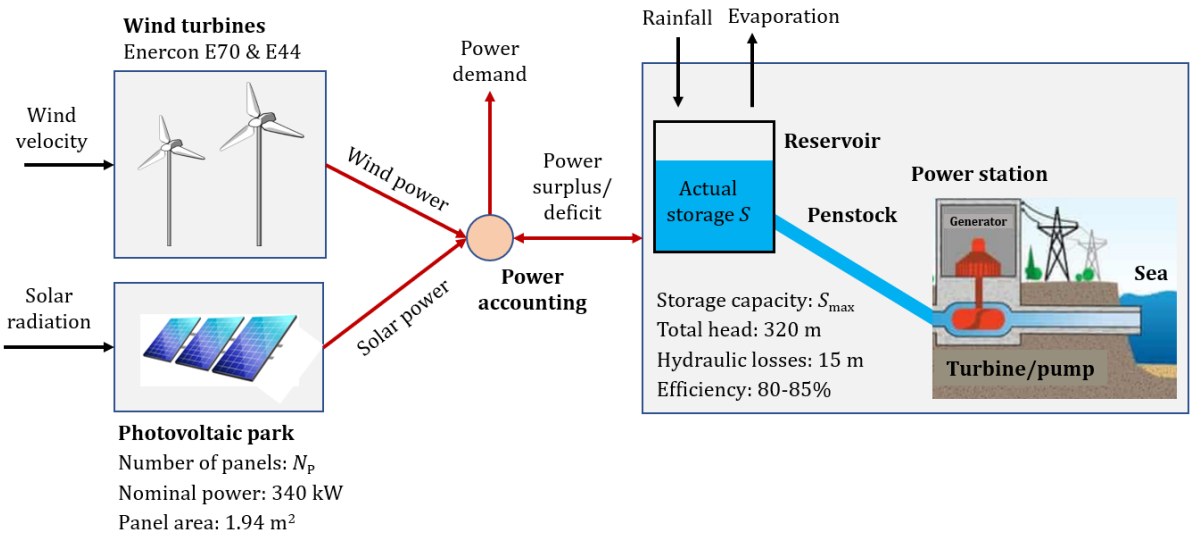

Εικόνα 2: Διάταξη προτεινόμενου υβριδικού συστήματος

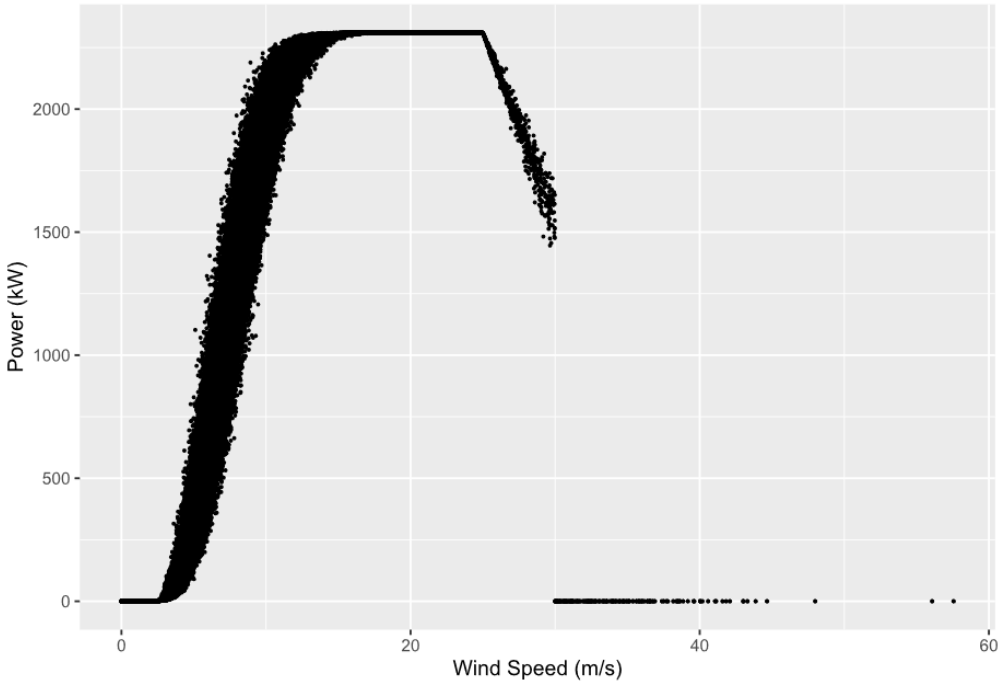

Εικόνα 3: Παράδειγμα προσομοιωμένης καμπύλης ανεμογεννήτριας

Ακολούθως, ορίζεται το πρόβλημα βελτιστοποίησης του υβριδικού συστήματος στο προγραμματιστικό περιβάλλον Rstudio. Οι παράμετροι του προβλήματος είναι το ωφέλιμο βάθος του ταμιευτήρα και το πλήθος των φωτοβολταϊκών. Η στοχική συνάρτηση αποσκοπεί στην μεγιστοποίηση του μέσου ετησίου κέρδους, επιτυγχάνοντας ταυτόχρονα υψηλή αξιοπιστία, αφού η αξιοπιστία έχει εκφραστεί σε όρους κέρδους στο πρόβλημά μας. Συγκεκριμένα, έχουν οριστεί οικονομικές ρήτρες που αποσκοπούν στην ελαχιστοποίηση τόσο της συχνότητας αστοχιών του συστήματος όσο και των ποσοτικών αστοχιών. Ως αστοχία συστήματος ορίζεται η μη κάλυψη των ενεργειακών αναγκών σε ένα χρονικό βήμα της προσομοίωσης. Ο εξελικτικός αλγόριθμος βελτιστοποίησης ακολουθεί το διάγραμμα ροής, όπως παρουσιάζεται στην **Εικόνα 4**.

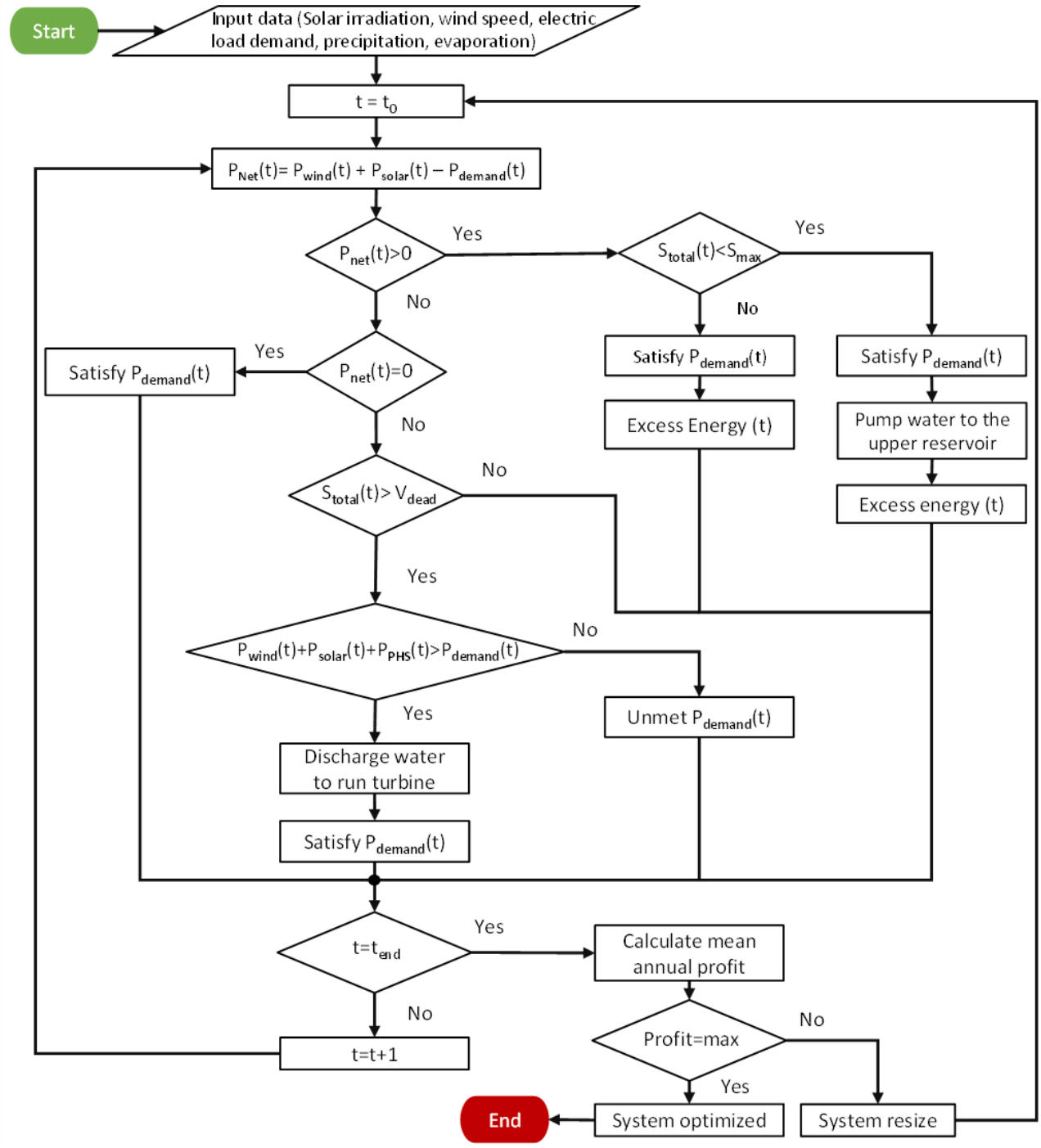

Εικόνα 4: Διάγραμμα ροής του προτεινόμενου μοντέλου βελτιστοποίησης του υβριδικού συστήματος

Για λόγους σύγκρισης, η βελτιστοποίηση πραγματοποιήθηκε στο προτεινόμενο σύστημα χωρίς αβεβαιότητα, και, στην συνέχεια, υπό καθεστώς αβεβαιότητας για 100 διαφορετικά σενάρια. Η **Εικόνα 5** παρουσιάζει την διακύμανση του αποθέματος του ταμιευτήρα κατά την διάρκεια της προσομοίωσης.

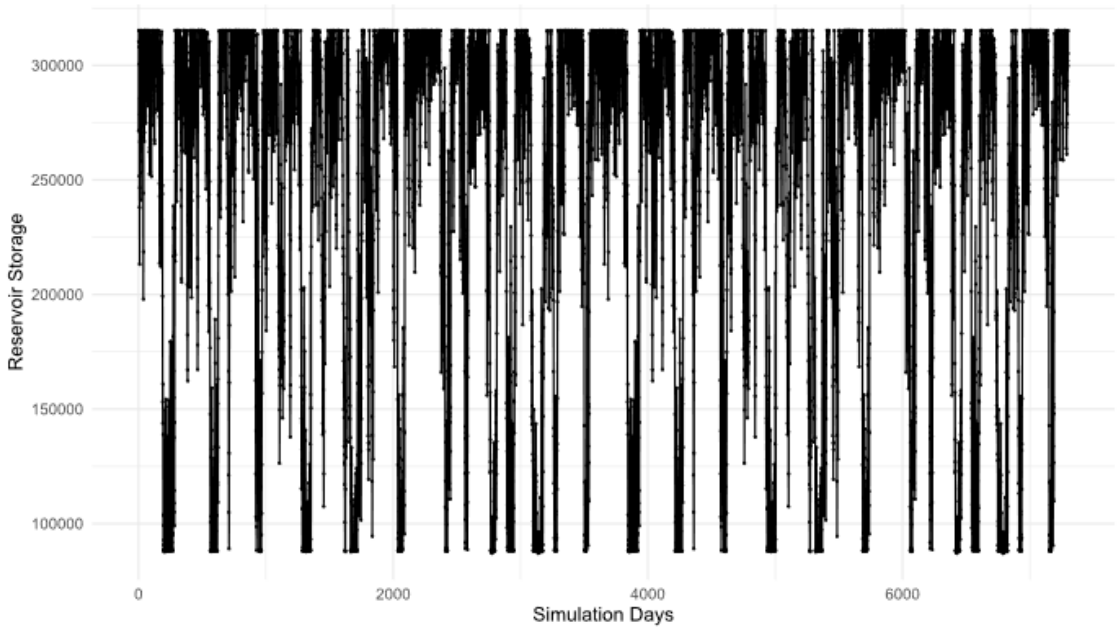

Εικόνα 5: Διακύμανση αποθέματος ταμιευτήρα κατά την προσομοίωση

Συγκρίνοντας τα αποτελέσματα, εξάγουμε τα παρακάτω συμπεράσματα:

- Το καθεστώς αβεβαιότητας στα βελτιστοποιημένα σενάρια προσδίδει αυξημένη διακύμανση στο μέγεθος το ταμιευτήρα, στην μέση ετήσια παραγωγή ενέργειας, στο μέσο ετήσιο όφελος και στην αξιοπιστία
- Όσο μεγαλύτερη η κλίμακα του έργου, ήτοι ο ταμιευτήρας και το πλήθος των φωτοβολταϊκών, τόσο μεγαλύτερη η αξιοπιστία του έργου. Ωστόσο, πρέπει να σημειωθεί ότι τα έργα μεγάλης κλίμακας παρουσιάζουν προβλήματα τεχνικής φύσεως όσον αφορά την κατασκευή και υλοποίηση.

Τέλος, συσχετίζουμε το κόστος με το ωφέλιμο βάθος το ταμιευτήρα μέσω γκαουσιανής πολυμεταβλητής κατανομής (copula) για να ποσοτικοποιήσουμε την αβεβαιότητα για εύρος τιμών σχεδιασμού (**Εικόνα 6**). Η κατανομή αυτή συσχετίζει το μέσο ετήσιο κέρδος με το ωφέλιμο βάθος του ταμιευτήρα και μπορεί να χρησιμοποιηθεί ως υποστηρικτικό εργαλείο λήψης αποφάσεων για τον σχεδιασμό υπό αβεβαιότητα.

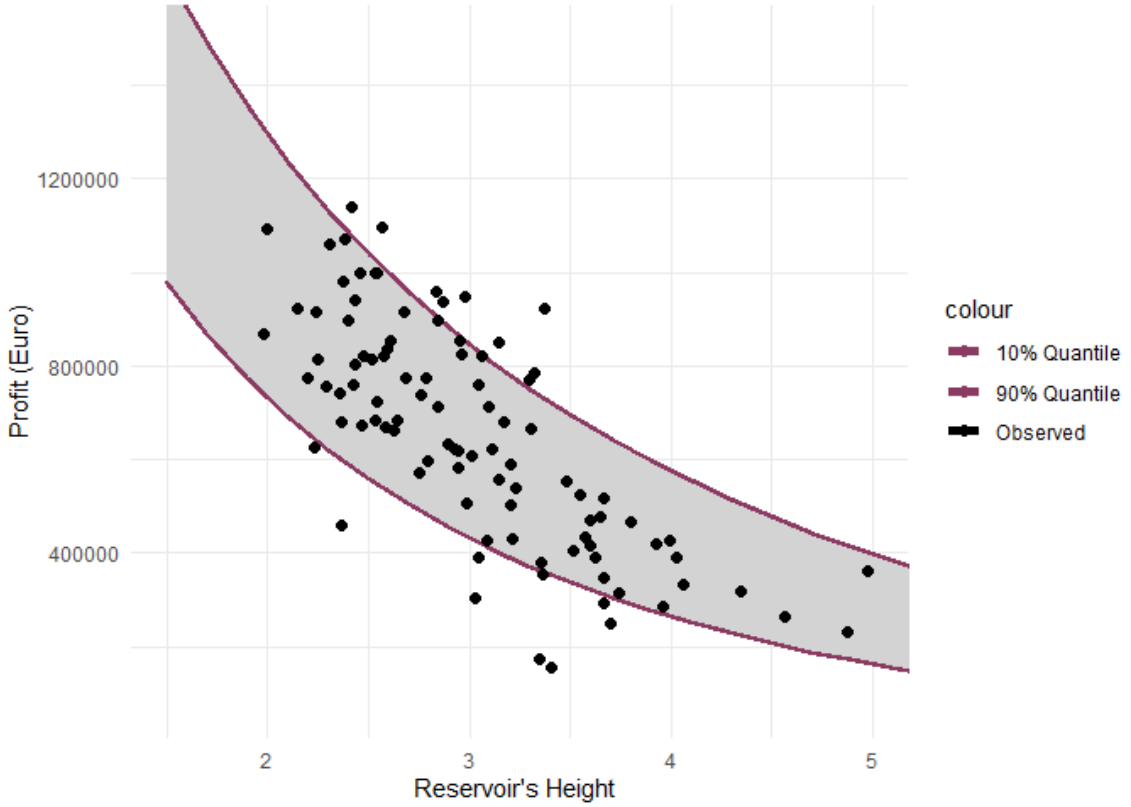

Εικόνα 6: Γκαουσιανή (Gaussian) copula για τη συσχέτιση μέσου ετήσιου κέρδους και ωφέλιμου ύψους ταμιευτήρα

1. Introduction

1.1 Incentive

In recent years, the continuously growing energy demand, in combination with unprecedented events, namely the armed conflict in Ukraine, have introduced significant issues in the energy supply. In parallel to this, climate change is imposing the shift from fossil fuels to renewables. Renewable energies, environmentally friendly and inexhaustible, are the mainstay of the effort to achieve the objectives set out in the Paris Agreement and the UN Sustainable Development Goals (SDGs), particularly those relating to the fight against climate change and universal access to energy.

The energy supply challenge mentioned above is even more significant in remote regions and areas that are not connected to the main energy grid (e.g., islands). The design of hybrid renewable energy systems (HRES) with energy storage systems can offer energy independence in such regions. However, multiple facets of uncertainty must be considered to ensure high reliability in covering the energy demand.

In this diploma thesis, we incorporate exogenous and endogenous uncertainties in designing and optimizing a hybrid renewable energy system with pumped seawater storage on the Greek island of Sifnos. A preliminary study of this system, only considering exogenous uncertainties, was presented at the General Assembly of the European Geosciences Union (Zisos *et al.,* 2022).

1.2 Research Objectives

The main research objectives of this thesis are outlined as follows:

- Provide a comprehensive overview of the components of a hybrid renewable energy system and their interdependencies;
- Present multiple facets of uncertainty to be incorporated into the suggested system;
- Outline the operation of the proposed HRES;
- Provide a holistic optimization approach of the proposed HRES under uncertainty;
- Outline the effects of uncertainty in HRES planning by comparing the optimized system to the initial deterministic approach.

1.3 Thesis Outline

This thesis is divided into eight chapters.

This **first chapter** introduces the subject of the thesis and its research objectives.

The **second chapter** provides an overview of hybrid renewable energy systems' components, with a focus on the implemented systems on Greek islands.

The **third chapter** includes a literature review of technological advances in HRES. Moreover, it addresses various facets of uncertainty (exogenous and endogenous) and outlines system optimization methods.

The **fourth chapter** presents the case study of Sifnos island, addressing technical challenges that arise from the design of the proposed HRES.

The **fifth chapter** simulates the operation of the HRES. It outlines the assumptions and methods in which uncertainty was incorporated and provides the system's evaluation method through economic data.

The **sixth chapter** presents how the simulated HRES was set up in the Rstudio environment. Moreover, the optimization method is analyzed under economic and reliability criteria.

The **seventh chapter** outlines the optimization results for the proposed HRES, with and without the incorporation of uncertainty.

The **eighth chapter** summarizes the thesis' conclusions and provides future research perspectives.

2. Overview of hybrid energy systems

2.1 About hybrid energy systems

Energy demand is continuously growing across the world as the population increases. If improvements in energy efficiency do not offset this increased demand, global energy consumption will continue to grow, making the challenge of transitioning energy systems away from fossil fuels and towards low-carbon energy sources more difficult. Figure 1 presents the evolution of primary energy consumption per capita (Our world in data, 2022).

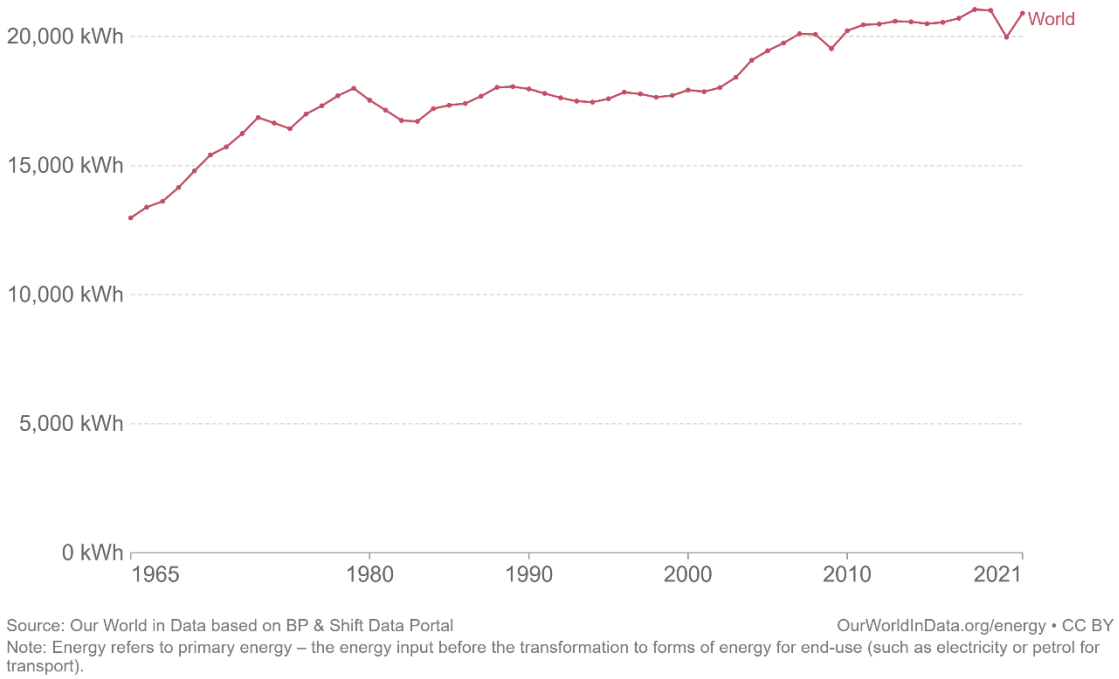

Figure 1: Evolution of primary energy consumption per capita

With regard to this, hybrid energy systems were first introduced in the 1970s. Hybrid energy systems generate electricity from two or more energy sources, usually renewable, sharing a single connection point. Combining renewable energy sources, namely wind, solar radiation, and hydraulic energy in hybrid installations, commonly complemented by storage systems, is an effective tool for delivering clean and efficient energy. Their potent advantage is the ability to switch between energy sources when one is insufficient, reducing the inherited unpredictability of renewables. Hybrid energy systems can also capitalize on existing energy infrastructure and add components to help reduce costs, environmental impacts, and system disruptions (J.J. Ding et al., 2000).

Planning a hybrid electricity system has a market focus rather than a technology focus: the priority is to choose the most fitting, efficient, and reliable mix of energy technologies to meet users'

needs. Thus, a unique design solution may be insufficient, as its layout and components depend on various highly uncertain variables, e.g., hydroclimatic cycle and energy conversion models.

2.2 Components of hybrid energy systems

Hybrid renewable-based energy systems (HRES) consist of at least two types of renewable energy sources, such as wind, solar, and hydropower, and an alternative source of power (e.g., diesel generator or fuel batteries) in case of emergency. An HRES may be connected to the main power station or have its own individual electricity generation system, as shown in Figure 2. The following sections provide a brief overview of each component of an HRES.

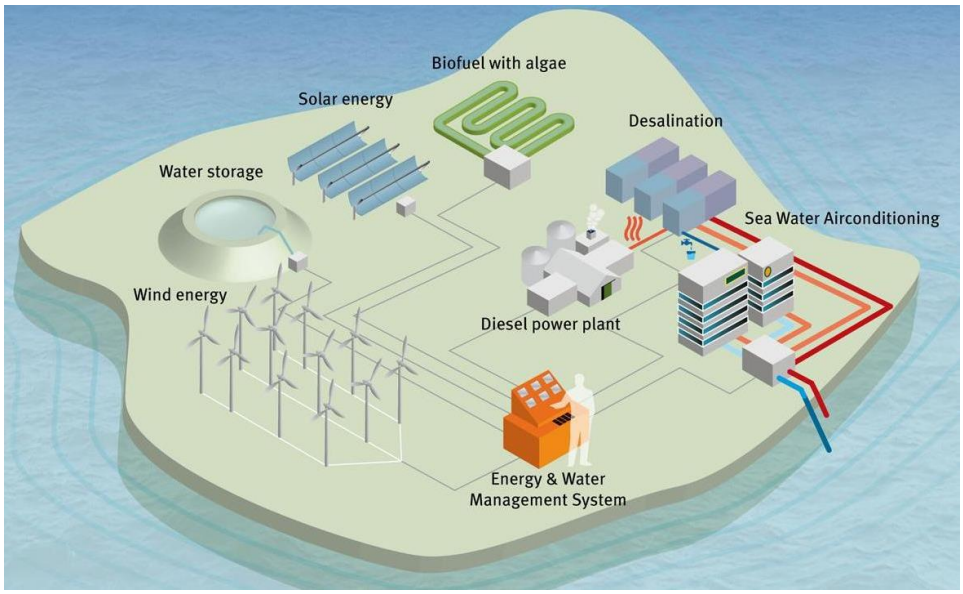

Figure 2: Example of an individual hybrid energy system

2.2.1 Wind turbines

Wind turbines are usually one of the main energy sources of an HRES. They are distinguished into two basic types: horizontal and vertical axis, with the former being the ones that are most commonly used. Wind turbines utilize wind speed values ranging between 2.5 and 25 m/s, transforming the wind's kinetic power into mechanical through the rotor blades and then from mechanical into electricity through the generator located in the hub of the tower, as depicted in Figure 3.

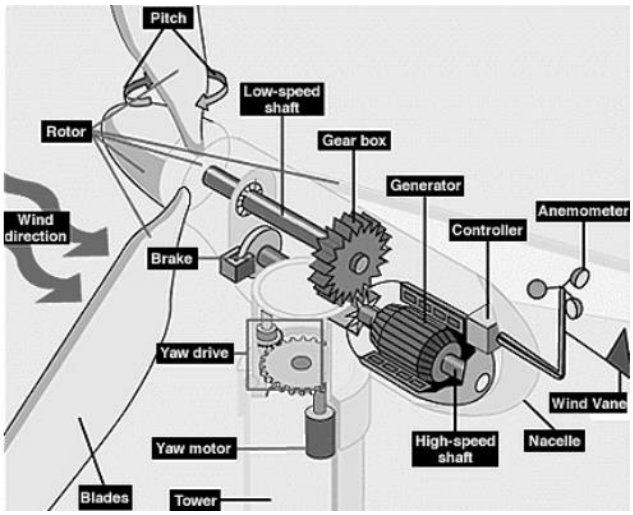

Figure 3: Components of a wind turbine

The produced power varies depending on the wind speed at the given time and the characteristics of each wind turbine (nominal power, hub height, rotor diameter). It is presented through the wind power curves provided by the manufacturers. In any case, the maximum available wind stream captured at a given time by a wind turbine equals 59.3%, known as the Betz limit.

2.2.2 Photovoltaics

Solar radiation is another indispensable renewable energy source exploited through photovoltaics. Photovoltaics (PV) generate electricity directly from sunlight through an electronic process that occurs naturally in certain types of material, the semiconductors. Photons strike and ionize semiconductor material on the solar panel, causing outer electrons to break free of their atomic bonds. Due to the semiconductor structure, the electrons are forced in one direction, creating a flow of electrical current. Solar cells are not fully efficient, as only certain light within the spectrum can be absorbed. Lastly, some of the light spectrum is reflected, while some is too weak to create electricity (infrared), and other (ultraviolet) creates heat energy instead of electricity. Figure 4 depicts the components of a PV module.

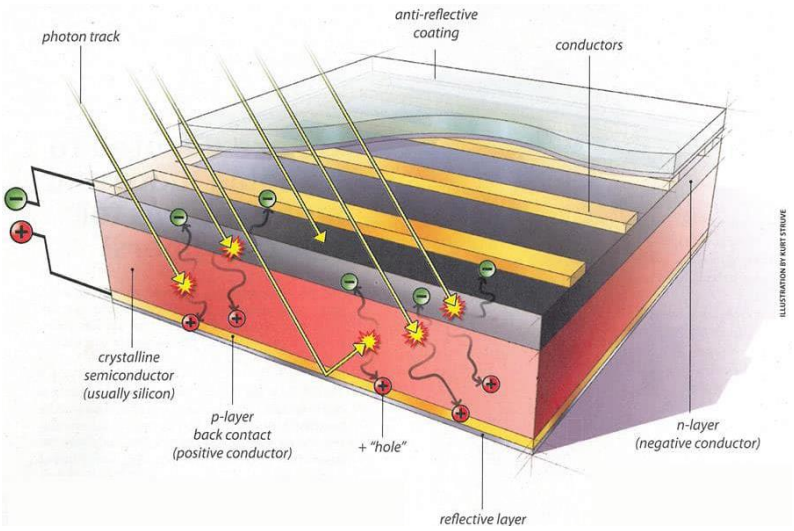

Figure 4: Diagram of a typical crystalline silicon solar cell (Solar Energy Industries Association)

The characteristics of a standard PV system, which is nonlinear, are demonstrated in Figure 5. The current versus voltage (I-V) curve differs based on if the PV array is in parallel, single, or as series.

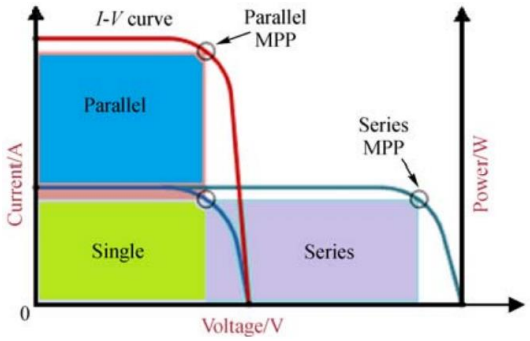

Figure 5: The I-V characteristics of a typical solar PV array (Faccio et al., 2018)

2.2.3 Pumped water storage

An electricity transmission and distribution system is unable to store significant quantities of energy. As demand rises and falls, so must the supply of electrical power to the grid too, either from a matching variation in the generation or through the use of storage as a buffer. In order to address excess electricity issue, HRES that are not connected to the main power grid have integrated pumped water storage systems in their configuration to avoid loss of energy surpluses. A typical layout of a pumped water storage system consists of two reservoirs whose elevation difference is of the order of hundreds of meters. Energy storage is expressed in terms of water storage. Thus, water is pumped into the upper reservoir when there are energy surpluses. During energy deficits, the two-reservoir system functions as a hydroelectric power station, exploiting the elevation difference to produce energy. Pumped water storage systems are highly reliable, as they have a rapid response time (from idle to full output in a time span of 20 seconds to a few minutes) (Blakers *et al.,* 2021). Their lifespan exceeds 50 years, with an overall efficiency ranging from 65% to 87%. As reported by the Electric Power Research Institute (EPRI) in 2017, they account for more than 96% of bulk storage capacity worldwide.

2.3 Layout and operation

Combining the aforementioned energy components in a proper layout of an HRES, an example is given in Figure 6; the system's operation is exclusively dependent on power demand. When the available renewable energy potential is sufficient to cover the energy demand at a given time, the surplus energy is utilized by pumping water from the lower reservoir to the upper. On the contrary, if the available renewable energy potential is insufficient to cover the energy demand, hydraulic energy is produced through the turbine by transferring water from the upper to the lower reservoir.

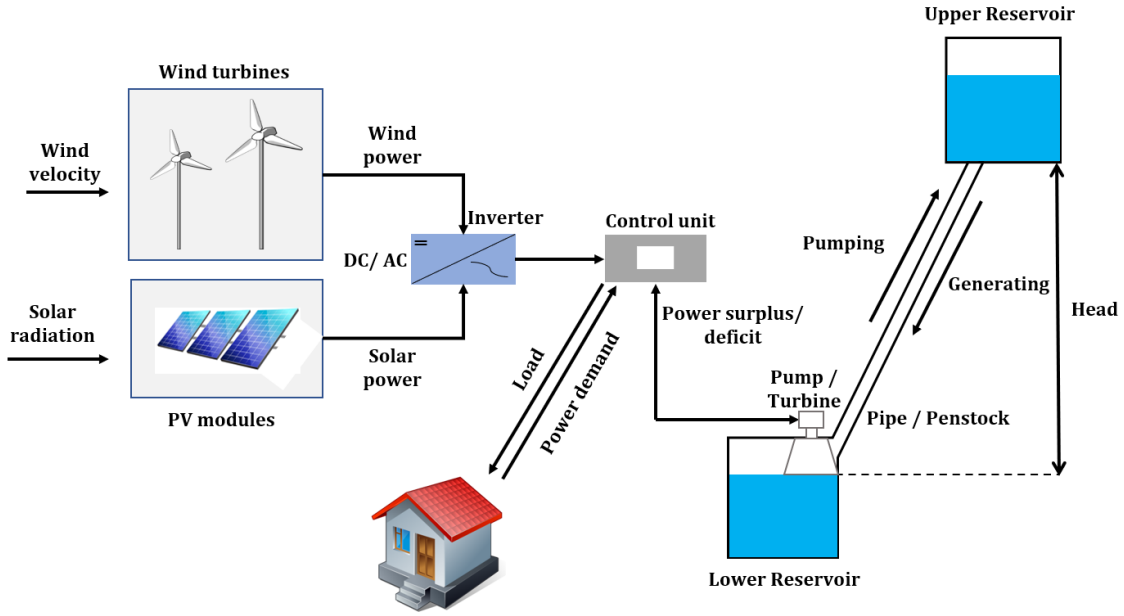

Figure 6: Typical layout of an HRES

2.4 Hybrid energy systems in Greek Islands

Large-scale energy storage is needed in regions with higher solar and wind penetration. It is also considered essential in regions and countries with weak or absent transmission links. Moreover, isolated island systems have felt this pressure even more strongly since they often face inflated fuel costs due to extra shipment costs and small overall system size. Greece consists of 227 inhabited islands (Hellenic Organization of Tourism, 2022) while also having 29 non-interconnected island systems (Zafeiratou & Spataru, 2019). Non-Interconnected Islands (NIIs) are those islands whose Electricity Distribution Network is not connected to the Transmission System or the Distribution Network of the mainland. Given that the islands' population increases significantly during the summer months, most NNIs fail to cover their peak power demand, leading to economic losses. Therefore, it is crucial to ensure their energy independence while taking advantage of their high renewable energy potential (wind and solar radiation). The importance of the integration of HRES in Greek islands was highlighted in the analysis performed on three Greek islands (Crete, Lesvos, and Serifos) by Caralis et al. (2010). The latter concluded that, apart from the environmental benefits of HRES, their development cost is competitive to the

fuel cost of local power stations in autonomous islands. A brief overview of hybrid energy systems in Greek islands follows:

2.4.1 Tilos island and HRES implementation

Tilos belongs to the complex of the Dodecanese islands with a population of 899 inhabitants (Hellenic Statistical Authority, 2021). Its hybrid energy system, which is a result of a Horizon 2020 project, started functioning in 2019 and consists of the following:

- A wind turbine of 800 kW nominal power
- Photovoltaics of 160 kW nominal power
- Inverters of 20 kW nominal power
- Battery arrays of 2.8 MWh power

The aforementioned system is capable of covering a minimum of 60 to 70% of the island's total energy needs.

2.4.2 Ikaria island and HRES implementation

Ikaria is an island in the eastern Aegean with a population of 10,175 inhabitants (Hellenic Statistical Authority, 2021). Its hybrid energy system, "Naeras" of 6.85 MW installed power, started functioning in 2019 and consists of the following sub-systems:

- A wind turbine park located on the hill "Stravokoudoura", including three wind turbines with 900 kW nominal power each.
- A small hydroelectric station with a turbine of 1.05 MW, exploiting the surplus water of the "Pezi" dam's reservoir, after ensuring that the water city's water supply needs and the environmental flow are met.
- A small hydroelectric station with two turbines of 3.1 MW total power, exploiting the surplus water of the pumped water storage.
- A pumped water storage consisting of two tanks of 80,000 m^3 volume each located in "Proespera" and "Kato Proespera" respectively, and a 910,000 m^3 volume reservoir in "Pezi".
- Pump station in "Kato Proespera" consisting of twelve-250 kW pumps

The projected annual energy production of "Naeras" is 9.80 GWh, while the annual reduction in CO_2 emissions is estimated at 13,800 tons (HEDNO).

2.4.3 Astypalaia and HRES implementation

Astypalaia is located in the Aegean Sea, with a population of 1,849 (Hellenic Statistical Authority, 2021). The island's energy needs are mainly covered by a diesel thermal station of 5.1 MW installed power. The annual share of renewables to the island's energy mix for 2019 was 8.4% (HEDNO, 2020), mainly derived from the photovoltaics 0.32 MW total power. A hybrid energy system for Astypalaia was proposed (Makris, 2021), consisting of 1.67 MW of photovoltaics, two wind turbines of 1.6 MW installed power, 2.04 MW Diesel generators, 2.1 MWh Li-ion batteries and 1.49 MW power converters. This system enables renewables to contribute to the island's annual energy share by 78.9% while also producing a 37.6% energy surplus.

3. Technological and research advances in hybrid energy systems

3.1 Literature review

Hybrid renewable energy systems have become an essential part of global energy production, addressing limitations in terms of fuel flexibility, efficiency, reliability, emissions, and economics (Bajpai & Dash, 2012). Power can be generated based on the demand at any particular site depending on the availability of resources, thus significantly reducing grid dependence. However, to achieve continuous and effective delivery of power, HRES must ensure that the communication system and the associated infrastructures of the subsystems are well-defined. To address this, Eltamaly *et al.* (2021) proposed an internet of things (IoT) based architecture for HRES, enabling monitoring of electrical, status, and environmental information and facilitating the communication between the subsystems.

During the past decades, there has been a significant number of studies supporting the use of pumped water storage in hybrid energy systems. Lundsager *et al.* (2014) noted that without an integrated large energy storage in the grid, namely a pumped water storage, a maximum of 80% wind penetration may be feasible for a 100-kW grid, decreasing dramatically as the size of the electricity grid increases, for as low as 20% for a 10-MW grid. Rehman *et al.* (2015) also mentioned that pumped water storage can address issues that emerge from the large integration of wind power into the electricity network, such as: (1) handling changes in network impedances due to wind farm connection to the grid and its effects on the remote control-signals, (2) handling of harmonics created by the addition of wind on the grid and (3) stability problems that may occur due to dynamics behaviors of wind farms connected to the grids.

In continuation to those mentioned above, studies have proven that integrating a pumped water storage can be more beneficial in remote HRES than installing batteries. Ruisheng *et al*. (2010) mentioned that there is a significant fluctuation in energy production due to the intermittent nature of renewable energy sources. This results in the reduction of the batteries' service life, as they remain in a loss power state for a long period of time. Moreover, Ali and Jang (2020) performed a study on an optimum design of an HRES on the island of Deokjeok-do, South Korea. In particular, two different systems were optimized based on: (a) the lowest possible Net Present Cost (NPC) and (b) the lowest possible Levelized Cost of Energy (LCOE). From the comparison of the results, they concluded that utilizing a pumped water storage, with the sea working as the lower reservoir, leads to a cheaper initial investment cost for both systems than using batteries as an energy storage system.

As mentioned in section 2.1, there is no single optimal HRES configuration. Therefore, an optimization method has to be implemented for the planning of every HRES. Faccio *et al.* (2018) classified the optimization goals into the following: (1) factors affecting load demand, (2) energy production scenarios, (3) factors affecting the system's grid during the optimization process, (4) reduction of environmental emissions, (5) voltage stability index and (6) breakeven grid extension distance. Nevertheless, it is understood that objective functions can contain more than one of these goals, depending on the requirements of each system, which happens to be the case in multiobjective optimizations (Das *et al.,* 2020).

3.2 Addressing issues of uncertainty

Uncertainty has been a long-lasting issue in the design and optimization of HRES, deriving from various drivers. Sakki *et al.* (2022) discriminated the uncertainties into two main categories; exogenous (external) and endogenous (internal), as they are presented in Figure 7. The former category mainly refers to the inherent uncertainty of the system's drivers, whereas the latter refers to conversion processes and underlying modeling assumptions. Following this, this research introduced a novel stochastic optimization framework that addresses multiple facets of uncertainty (e.g., hydrometeorological parameters and the market price of energy). This framework will be the fundamentals for this thesis since we expanded from the single renewable-based work to a hybrid energy system.

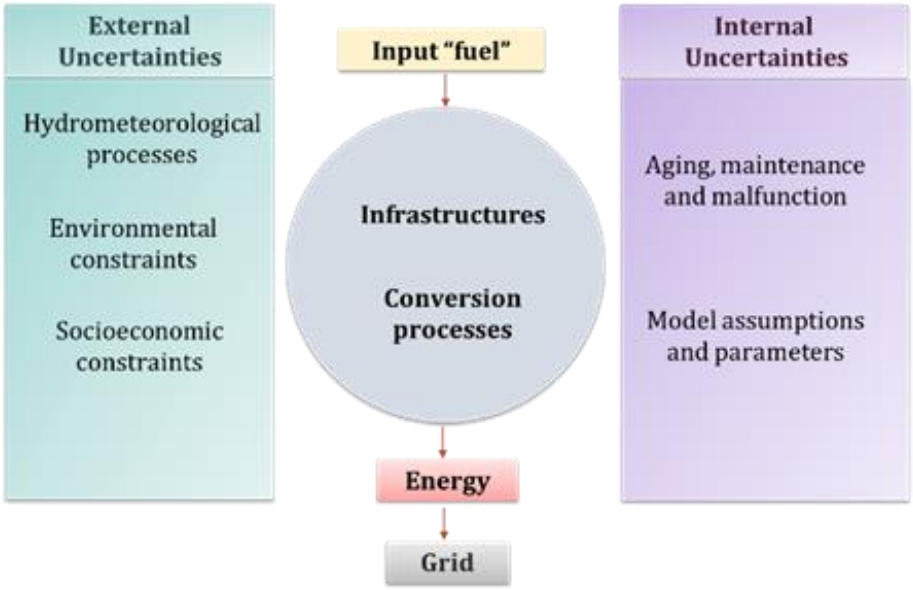

Figure 7: Key sources of uncertainty associated with renewable energy (Sakki et al., 2022)

3.2.1 Exogenous Uncertainties

Hydrometeorological processes are considered one of the main exogenous uncertainties of an HRES due to the intermittent nature of renewables. Hydrometeorological time series of lower time scales (e.g., monthly or daily) were found to be appropriately represented through theoretical distribution functions. Specifically, the Weibull and Gamma distribution have been considered appropriate to represent wind speed data (Carta *et al.,* 2009 and Zhou *et al.,* 2010), while the Beta distribution provides satisfactory fit in sunshine duration data (Bashahu & Nsabimana, 2005). In this context, Tsekouras & Koutsoyannis (2013) performed a comprehensive analysis on hydrometeorological data and their corresponding distributions to detect possible long-term persistence. In more recent studies, Tsoukalas *et al.* (2020) presented a simplified synthetic data generation procedure (for reproducing the hydrometeorological regimes) through anySim, an R-package specifically designed to simulate non-Gaussian correlated random variables, stochastic processes at single and multiple temporal scales, and random fields. Following this, Palma *et al.* (2021) presented a novel methodology to facilitate the selection of a

proper time series generation model for renewable energy sources, providing a set of indicators to verify the selected model's accuracy.

Another exogenous uncertainty that should be taken into consideration is the energy demand. Energy demand can be affected by various factors, such as environmental and socioeconomic (Abdel-Aal, 2008). A study conducted by Cabeza *et al.* (2018) showed that past energy projections for the energy demand of OECD countries were either consistently overestimated or underestimated. This phenomenon intensifies even more in the islands due to the intensive seasonal power demand variations. Thus, it is essential to accurately forecast energy demand while designing an HRES. Warren *et al.* (2016) introduced a generalized mathematical framework for uncertainty forecasting and then examined three main constituents of uncertainty in energy demand forecasts; (1) inherent randomness in the way electricity is consumed, (2) modeling and estimation errors, and (3) uncertainty in the model inputs. Islam *et al.* (2020) presented various models for short, medium, and long-term energy demand forecasting and metrics to measure their accuracy effectively.

3.2.2 Endogenous Uncertainties

Uncertainty in power system operations can be categorized between discrete and continuous disturbances (Papavasiliou *et al.*, 2015). The discrete disturbances to equipment failure, such as generators and transmission lines, were accurately demonstrated in an analysis performed on wind turbine generators by Rezamand *et al.* (2019). The results showed that the reliability of wind turbine generators (WTGs) can decline to as low as 67.9% after seven years of operation. The continuous disturbances, which include parameters of the unit commitment problem that vary smoothly (e.g., electricity demand and renewable power production), were described in the previous section.

As the penetration of wind power in renewable energy systems increases, concerns about the uncertainty in wind power generation are raised. Another type of uncertainty to be considered is found in wind turbine power curves (WTPC). A WTPC, provided by the manufacturer, gives a wind turbine's standard and experimental behavior as a graph or as a set of points for wind speed – power every 0.5 m/s (Villanueva & Feijóo, 2018). However, a wind turbine operates in complex and variable conditions, which deviate significantly from the stable experimental conditions under which manufacturers test them. Thus, the provided WTPC does not accurately reproduce the actual behavior of wind turbines that operate in the real-world (Pagnini *et al.*, 2015). For this reason, ample deterministic and probabilistic models were developed to produce a WTPC that resembles real-world operating conditions. Recently, the focus has been shifted towards the latter since deterministic models provide fixed relationships between wind speed and power generation, failing to reveal the variating and dynamic power generation process (Kusiak *et al.*, 2009). A novel probabilistic WTPC model worth mentioning is the one developed by Yan *et al.* (2019), which considers various model inputs (pitch angle, wind direction) based on three non-parametric algorithms.

The last, but not least, issue of uncertainty involves the operation of wind turbines in the high wind speed region. It is impossible to accurately predict when the wind turbines will shut down and their downtime, which occurs when wind speed exceeds the value of 25 m/s, due to the stochastic nature of wind (Petrović & Bottasso, 2014). Thus, to prevent frequent shutdowns and

restarts, the soft cut-out strategy is implemented by extending the maximum admissible wind speed up to 30-32 m/s, without an abrupt shutdown, through controlling pitch and generator in order to decrease the energy production slowly (Catellani *et al.*, 2019). Multiple studies have addressed the optimal control of wind turbines during high wind speeds to minimize the uncertainties derived from the wind. Jelavic *et al.* (2013). produced a soft-cut out strategy worst-case scenario algorithm that does not significantly increase fatigue loads. Astolfi *et al.* (2018) performed a SCADA data analysis, extending the power curve of a wind turbine farm in the high-speed region, and concluded that the simulated energy improvement was 0.62%, namely 1.80% of the wind farm's total production. Lastly, Castellani *et al.* (2019) extracted operational data from a 2.3 MW wind turbine. They then simulated it to work with the soft cut-out strategy, producing 1.02 MW more than its initial operating state.

4. Case study

4.1 General Information

The under-scope case study concerns the island of Sifnos. Sifnos is located in the southern region of the Cycladic complex between Serifos and Kimolos. Its area extends to 74 km^2, and its coastline is 70 km^2 long. Its morphology consists mainly of hills and fruitful valleys, with its primary geological formation being the dolomitic marble. The permanent population of Sifnos is 2,755 (Hellenic Statistical Authority, 2021), while the island attracts up to 100,000 tourists every summer.

Sifnos is a non-interconnected island (NII). Its energy production is mainly covered by a 9.0 MW oil power station, while renewables have a small share in the total annual energy mix. Specifically, there is a small 1,2 MW wind park and two photovoltaic parks of 0,203 MW power (excluding the photovoltaics on the rooftops of the houses). According to an analysis of the island's energy profile for 2020, the total energy demand was 17,30 GWh, while the peak was 5,40 MW, occurring during the summer months (HEDNO, 2021).

4.2 Proposed system outline

A preliminary study for this system was performed by Katsaprakakis and Voumvoulakis (2018). The HRES they proposed combines wind, solar and hydroelectric energy. A major component of the proposed layout is the pumped-storage system. Due to the limited surface water resources of the island, an upper reservoir is configured at an elevation of 320 m, recycling seawater. The HRES will be installed on a plateau located on the island's northern part, as shown in Figure 8.

Figure 8: Location of the proposed HRES

The selected location is ideal since:

- The intervention to the natural environment is minimal, as there are no tourist attractions or human activities nearby, with the nearest settlement situated at a distance greater than 4 km away.
- The mild topography of the plateau and the slope minimize the required excavations effort and, thus, cost.
- There is high wind potential, as there are no physical obstacles in the island's northern part.

Following the initial design concept, Figure 9 provides a more detailed overview of the system we propose and the interdependency of its sub-systems, as well as its key metrics. Meteorological parameters produce power through renewable energy modules (wind turbines, photovoltaics). The power accounting between produced energy and energy demand determines whether the seawater pumped storage will store excess energy by pumping water into the reservoir or produce energy to cover the deficits.

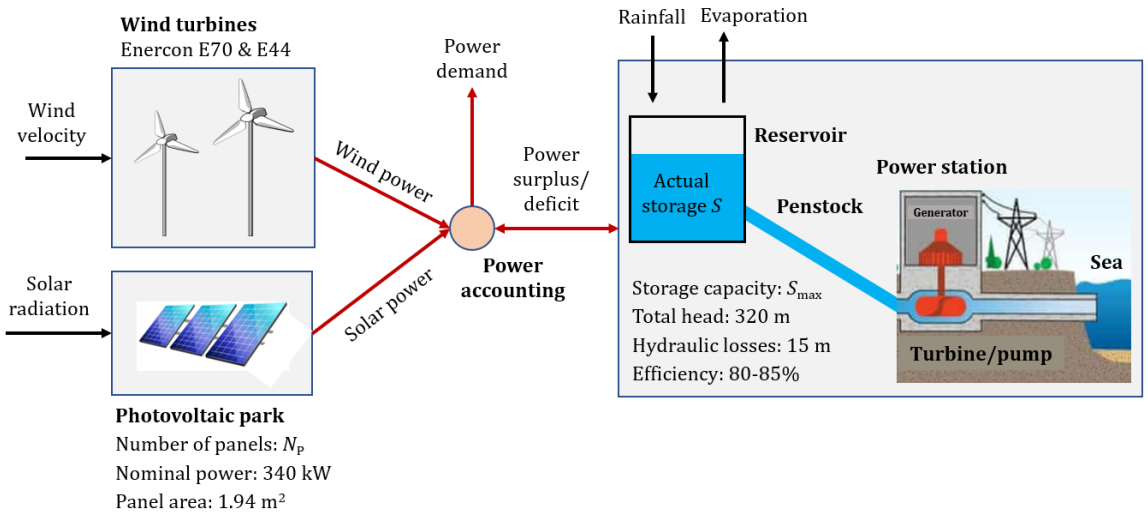

Figure 9: Proposed hybrid power system (Zisos et al., 2022)

4.3 Overcoming technical challenges

The inclusion of a seawater pumped storage in the HRES introduces various technical challenges. This section aims to address the most crucial ones, ensuring the proposed system's feasibility.

4.3.1 Erosion of the pipes

The erosion of the pipes due to the salt water is one of the main technical challenges. To address this, GRP pipes will be used. Glass(fiber) Reinforced Plastic (GRP) is a composite material that consists of a polymer matrix and glass fibers. The polymer matrix is usually an epoxy, vinyl ester, or polyester thermosetting resin, which brings environmental and chemical resistance to the product, acting as a binder for the fibers. The glass fibers add strength to the composite. GRP pipes are composed of a liner layer, an inner reinforced layer, a core layer, an outer reinforced layer, and a surface veil, as shown in Figure 10.

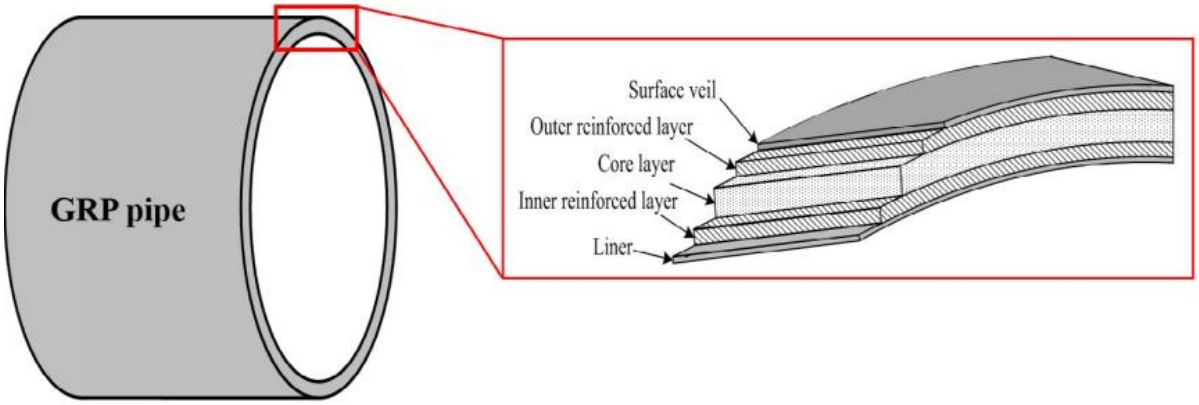

Figure 10: Configuration of a GRP pipe (Yoon and Oh, 2015)

Their main advantages include high resistance against chemicals, corrosion, UV radiation and long-life expectancy. Their low friction coefficient is befitting to address the potential issues of erosion and rugosity raised using seawater.

4.3.2 Erosion of the electromechanical equipment

Similar to the erosion of pipes, the erosion of electromechanical equipment poses another technical challenge. In their study, Francis and Hebdon (2015) found that several types of corrosion from seawater can affect stainless steel (SS) electromechanical equipment:

- Crevice corrosion is the most common form of corrosion initiated by changes in local chemistry within a crevice. It is usually associated with a stagnant solution in the microenvironments that tend to occur in crevices. In a seawater pump, crevices can be found where seals and impellers are fastened to the shaft, and flange faces are cast in for pipework connections.
- Erosion corrosion can happen because of the high velocity of seawater in a pump.
- Cavitation occurs when a fluid's operational pressure drops below its vapor pressure and causes gas pockets and bubbles to form and collapse. This common phenomenon occurs when a pump operates outside its normal design parameters. The formed bubbles erode the steel.
- Corrosion fatigue derives from the combination of alternating or cycling stresses in a corrosive environment, mainly affecting seawater pump shafts.

Table 1 was provided by Francis and Hebdon, containing the most common SS alloys that increase its resistance to corrosion in seawater. In the last column, the pitting resistance equivalent number (PREN) is calculated based on the nominal composition of each material according to the following equation:

$$PREN = \%Cr + 3.3 * (\%\, Mo + 0.5 * \%W) + 16 * \%N \qquad (4.1)$$

Table 1: Nominal Composition of some commonly used cast Stainless Steels (Francis & Hebdon, 2015)

			Nominal Composition (wt%)							
Type	UNS No.	Generic name	Fe	Cr	Ni	Mo	N	Cu	W	PREN
Austenitic	J92900	316	Bal	18	10	2	--	--	--	24
	J94651	CN3MN	Bal	20	24	6	0.2	--	--	43
	J93254	CK3MCuN	Bal	20	18	6	0.2	0.7	--	43
Duplex	J93372	Grade 1B*	Bal	25	5	2	0.14	--	--	34
	J92205	Grade 4A*	Bal	22	5.5	3	0.16	--	--	35
	J93404	Grade 5A*	Bal	25	7	4	0.3	--	--	41
	J93380	Grade 6A*	Bal	25	8	3.5	0.25	0.7	0.7	41
Bal = Balance										
Grade designations in ASTM A995										

Lastly, the NORSOK (Norwegian shelf's competitive position) standards state that SS with a PREN value of 40 is considered sufficient for equipment used in seawater.

4.3.3 Waterproofing of the reservoir

The waterproofing of the reservoir is considered essential while dealing with seawater. This measure is implemented to avert groundwater salinization by preventing the sea water's intrusion in the potentially karstified underlying geological formation. The waterproofing is achieved by installing High-Density Polyethylene (HDPE) Geomembranes, which have increased durability to chemicals and UV radiation.

5. Hybrid energy system simulation

5.1 Input data

The proposed hybrid energy system consists of multiple segments (Figure 9). In this section, we configure a model to simulate the operation of the HRES and define the interdependencies of its sub-systems. The simulation was performed in an hourly time step.

5.1.1 Solar power

The proposed system includes photovoltaics of rated 340 W rated power and 1.94 m^2 panel surface. The total energy produced is calculated by the following equation:

$$P_{solar} = N_{Panel} * W * A_{panel} \quad (5.1)$$

where:

N_{Panel} is the number of photovoltaic panels;

W is the solar radiation at a given time (W/m^2);

A_{panel} is the surface of the photovoltaic panel (m^2).

The solar radiation data for the island of Sifnos were provided by the National Observatory as an hourly step time series. Figure 11 indicates the produced power of the PV module for different values of solar radiation. When the solar radiation values exceed 1,000 W/m^2, the module produces its nominal power.

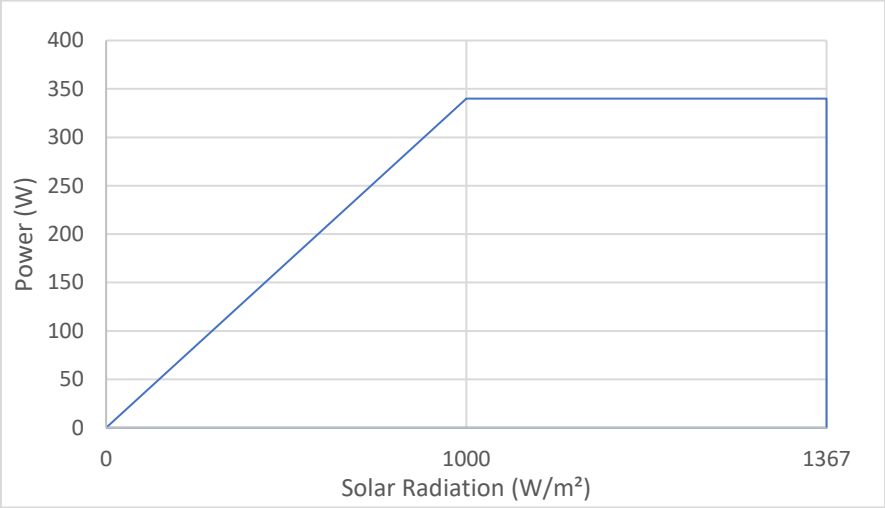

Figure 11: Power - Solar radiation plot of the PV module

5.1.2 Wind power

Two different wind turbines are included in the system to maximize the utilization of the available wind potential. Their key specifications are summarized in Table 2:

Table 2: Wind turbine specifications

Wind turbine type	Enercon E-44	Enercon E-70 E4
Rated power	900,0 kW	2.300,0 kW
Minimum power	4 kW	2 kW
Cut-in wind speed	3,0 m/s	2,5 m/s
Rated wind speed	16,50 m/s	15,0 m/s
Cut-out wind speed	34,0 m/s	34,0 m/s
Survival wind speed	59,50 m/s	-
Tower height	55 m	113 m
Rotor		
Diameter	44,0 m	71,0 m
Swept area	1.521 m²	3959 m²
Number of blades	3	3
Power density 1	591,7 W/m^2	581 W/m^2
Power density 2	1,7 m^2/kW	1,7 m^2/kW
Generator		
Voltage	690 V	2.000 V
Grid frequency	50 Hz	50 Hz

The wind speed data for the island of Sifnos were provided by the National Observatory as an hourly step time series. The anemometer that recorded those measurements is situated at a different elevation (5 m from sea level) than the hub of the wind turbines. Thus, the initial wind speed has to be calculated at the respective heights of each wind turbine hub, given that they are installed on the aforementioned plateau of 320 m elevation, according to the following equation:

$$u_2 = u_1 \left(\frac{\ln\left(\frac{z_2}{z_0}\right)}{\ln\left(\frac{z_1}{z_0}\right)} \right) \tag{5.2}$$

where:

u_2 is the wind speed at the wind turbine hub (m/s);

u_1 is the measured wind speed of the anemometer (m/s);

z_1 is the height of the measured wind speed (m);

z_2 is the height of the wind turbine hub (m);

z_0 is a surface roughness parameter (m), considered equal to 2 cm (crops of 10-50 cm) for our case study.

In addition, the wind component of HRES concludes wind turbines, Enercon turbines, i.e., Enercon E-44 and E-70 E4, with rated power 900 and 2300 kW, respectively. Figure 12 and Figure 13 depict the manufacturer power curves for the two wind turbines of the proposed HRES.

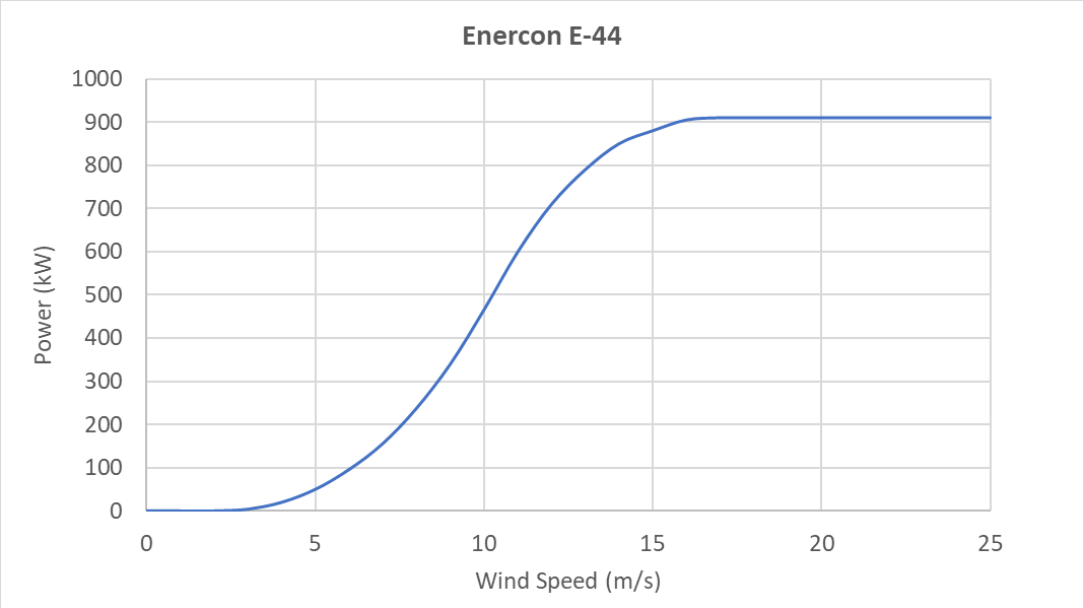

Figure 12: Power curve of Enercon E-44

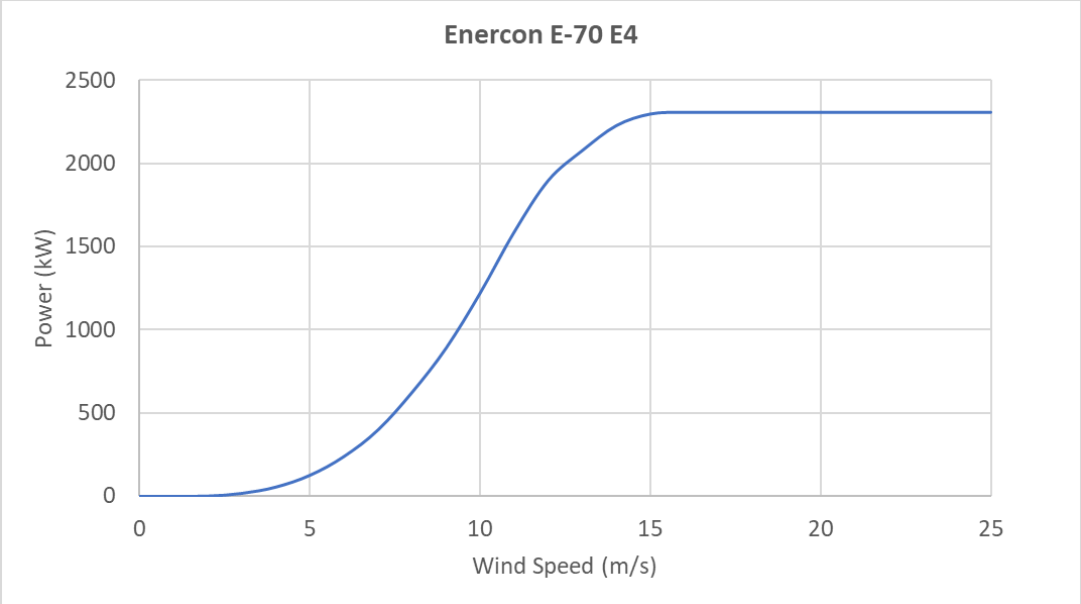

Figure 13: Power curve of Enercon E-70 E4

In order to calculate the power production of a wind turbine for a given wind speed value, an analytical formula introduced by Sakki *et al.* is chosen:

$$P_{wind} = P_{\min} + \left(1 - \left(1 - \left(\frac{V_{wind} - V_{min}}{V_{max} - V_{min}}\right)^{a}\right)^{b}\right)(P_{max} - P_{min}) \quad (5.3)$$

where:

$P_{\min}$ is the minimum power produced (kW);

P_{max} is the nominal power of the wind turbine(kW);

V_{wind} is the wind speed at the wind turbine hub (m/s) (for values exceeding 25 m/s, equation 5.7 is used instead);

V_{min} is the cut-in wind speed (m/s);

V_{max} is the cut-off wind speed (m/s);

a, b are shape parameters.

It is important to mention that equation 5.3, unlike the ones commonly used in other studies, is not a high order polynomial formula, since it takes into account turbine-specific characteristics and two parameters.

Since the proposed HRES consists of different hub-height wind turbines, it is expected that the interaction between large and small wind turbines (e.g., due to turbulence effects) will reduce the wind speed for the latter. The wind speed reduction is calculated as follows (Vasel-Be-Hagh & Archer, 2017):

$$V_{wind} = V_0\left(1 - \frac{2a}{\left(1 + \frac{2kL}{D_L}\right)^2}\right) \quad (5.4)$$

where:

V_0 is the freestream wind speed at the hub height level (m/s);

k is the decay coefficient;

a is the induction factor;

L is the distance between the wind turbines (m);

D_L is the diameter of the large turbine (m).

In the study of Vasel-Be-Hagh & Archer (2017), it is proposed that k = 0.038 and a= 0.1, which are the values that will be used for this case study.

5.1.3 Pumped water storage

The conventional pumped water storage consists of two reservoirs. For the proposed system layout, the lower "reservoir" is the sea, whereas the upper reservoir is trapezoid-shaped. Its key dimensions are depicted in following the cross sections (Figure 14 & Figure 15) and are in line with the exploitable plateau.

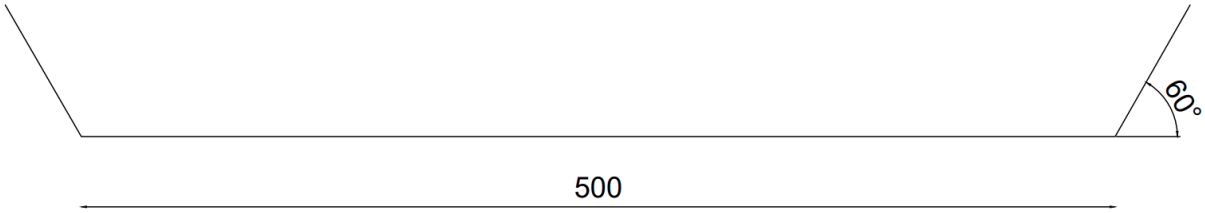

Figure 14: Cross section of the reservoir (parallel to the plateau)

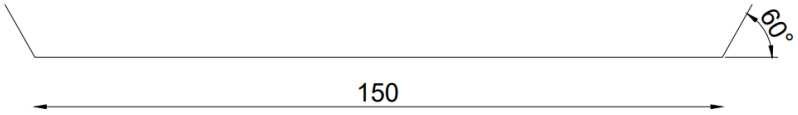

Figure 15: Cross section of the reservoir (perpendicular to the plateau)

By defining the reservoir's dimensions, we can calculate the reservoir's volume and surface area depending on its depth at a given time through the following formulas:

$$V(m^3) = 78{,}793H - 6{,}280.5 \tag{5.5}$$

$$A(m^2) = 763.89H + 74{,}978 \tag{5.6}$$

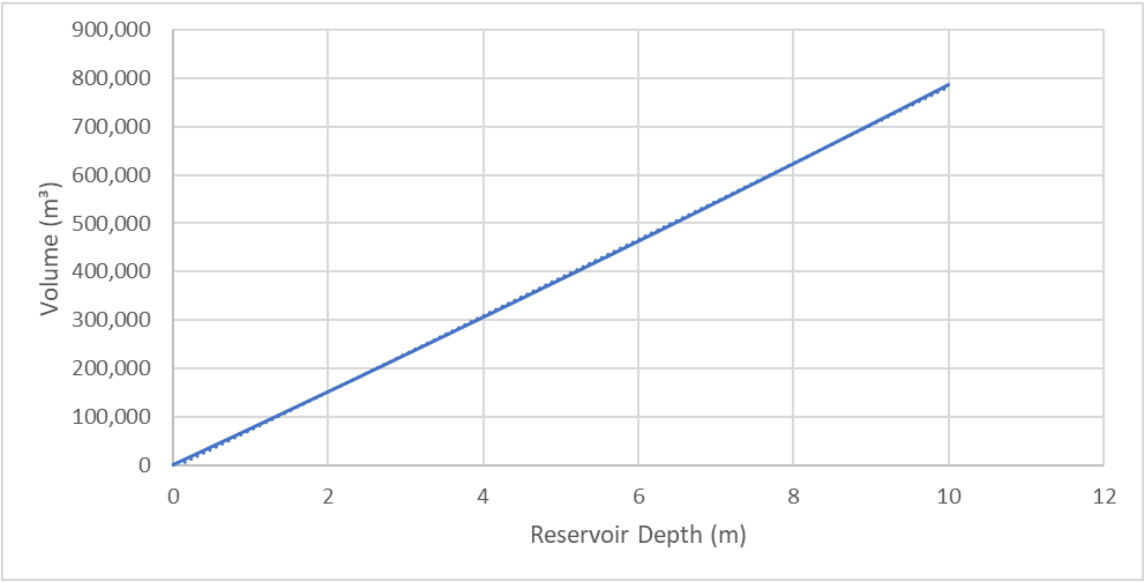

Figure 16: Volume - Reservoir Depth chart

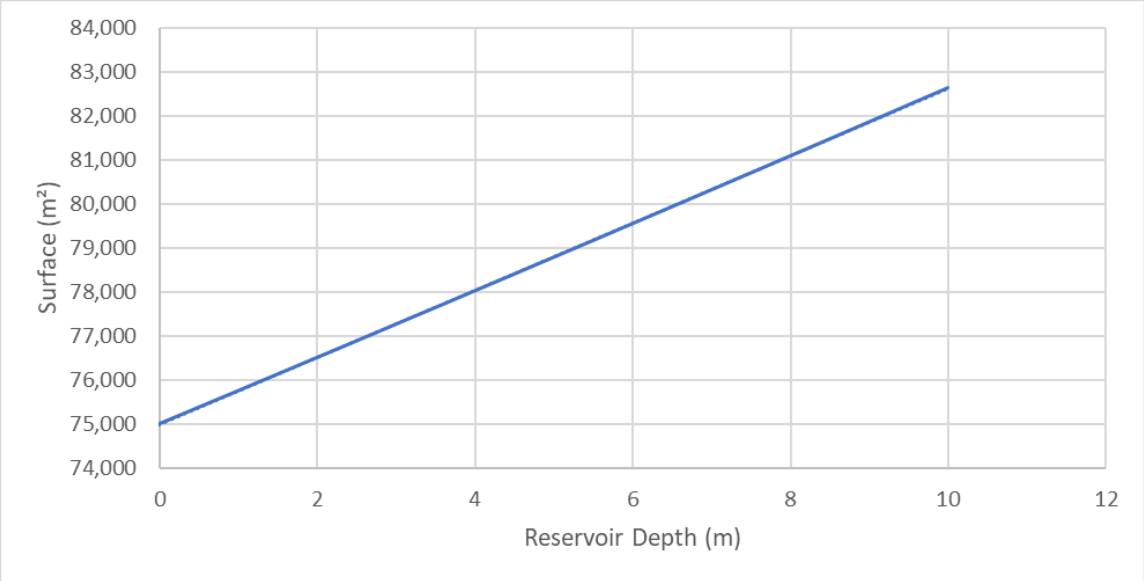

Figure 17: Surface area - Reservoir Depth chart

5.1.3.1 Reservoir inflows and outflows

The reservoir inflows and outflows considered in this case study are precipitation and evaporation, respectively. These data were extracted by the Hellenic National Meteorological Service's station in Naxos (daily measurements), then disaggregated on an hourly scale through the Hydrognomon software.

5.2 Simulation assumptions

This section aims to outline all the assumptions that were made to simulate the operation of the proposed HRES:

- The height of the intake is 1.2 m, leaving sufficient space as dead volume;
- The efficiency of the turbine and pump is 0.85 and 0.80, respectively;
- Hydraulic losses account for 5% of the total head;
- Due to the limited space of the plateau and to avoid under-exploitation of the wind turbines, four are selected for this case study (two large and two small);
- The distance between the wind turbines is 400 m;
- The penstock's length and diameter are 910 m and 1 m, respectively;

The number of photovoltaic modules and the reservoir's height are parameters that will be determined through the system's optimization.

5.2.1 Incorporating uncertainty in the simulation-optimization procedure

This thesis' main goal is to underline the importance of uncertainty while designing an HRES. The majority of uncertainties outlined in section 3.2 are included in the design optimization process, namely the hydrometeorological series, the wind turbine manufacturer power curve, and the wind turbine soft cut-out strategy. By incorporating multiple facets of uncertainty, we provide a holistic view of a hybrid renewable energy system's optimization.

5.2.1.1 Wind turbine power curve

As mentioned in section 3.2.2, the manufacturer's wind power curve derives from testing wind turbines under stable experimental conditions. By adding endogenous uncertainty, we better resemble on-site wind turbine behavior. To achieve this, we consider that the shape parameters of equation 5.3 are random variables. Specifically:

- $a \sim N(2.25, 0.0225)$
- $b \sim N(20, 0.016)$

These parameters were defined so that the simulated power curve's total average variation is no greater than 15% compared to the manufacturers'. It is an acceptable variation, considering that Lira *et al.* (2016) stated that power curve uncertainty is approximately 10%.

Moreover, the soft cut-out strategy is implemented to extend the power curves past the usual cut-out speed (25 m/s). Enercon implements the "storm control" strategy for the operation of its wind turbines in the high-speed region, stating, "*the rated speed is linearly reduced starting at a predetermined wind speed for each turbine type. Beginning at another turbine-specific wind speed, the limitation of the turbine's rated speed also reduces active power. The turbine only shuts down at a wind speed of more than 34 m/s (10-minute average)*". Figure 18 depicts the storm control strategy, where V1 is the cut-in wind speed, V2 is the rated wind speed, V3 is the beginning of power reduction, and V4 is the cut-out storm control wind speed.

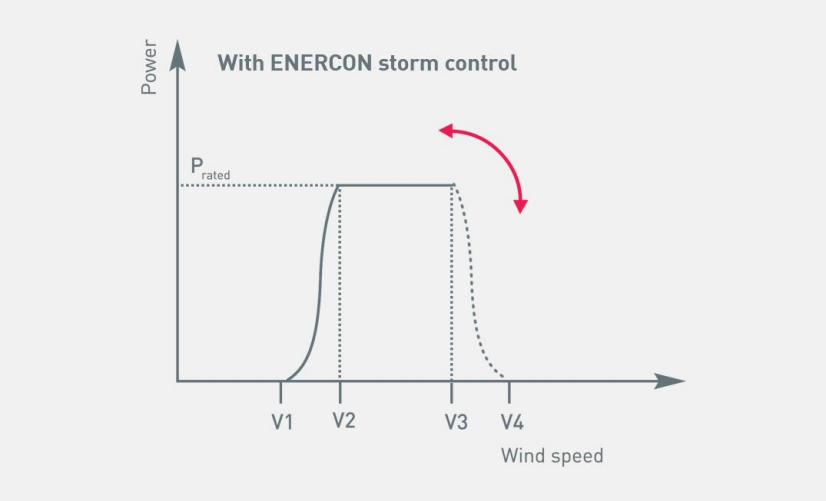

Figure 18: Enercon storm control for wind turbine behavior in the high-wind speed region

To calculate the produced power of the wind turbines in the high-speed region (where ramp control occurs), we assume the following formula:

$$P_{wind} = P_{max} - a(V - V_{cut-out}) \tag{5.7}$$

where,

P_{max} is the wind turbine's nominal power (kW);

$V_{cut-out}$ is the cut-out wind speed (25 m/s);

V is the given wind speed, ranging from 25-30 m/s;

a is the slope.

Similar to those mentioned above, we consider the slope a random variable to reproduce on-site wind turbine behavior more accurately. Specifically:

- $a \sim N(150, 225)$ for the large turbines
- $a \sim N(45, 100)$ for the small turbines

Figure 19 & Figure 20 depict an example of the simulated power curves for each wind turbine.

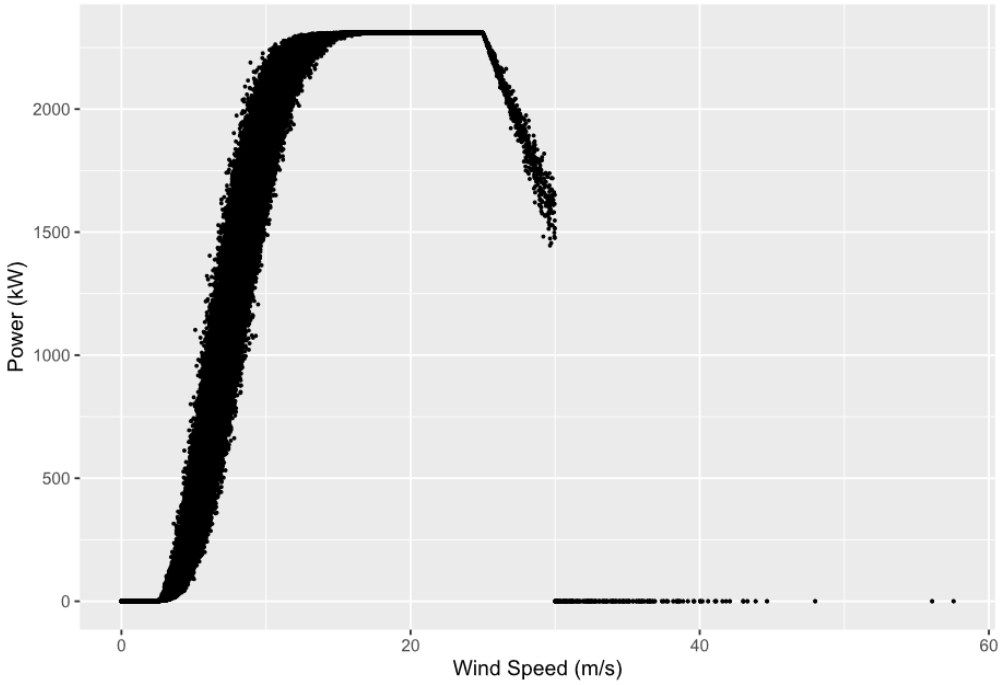

Figure 19: Example of a simulated power curve for Enercon E-44

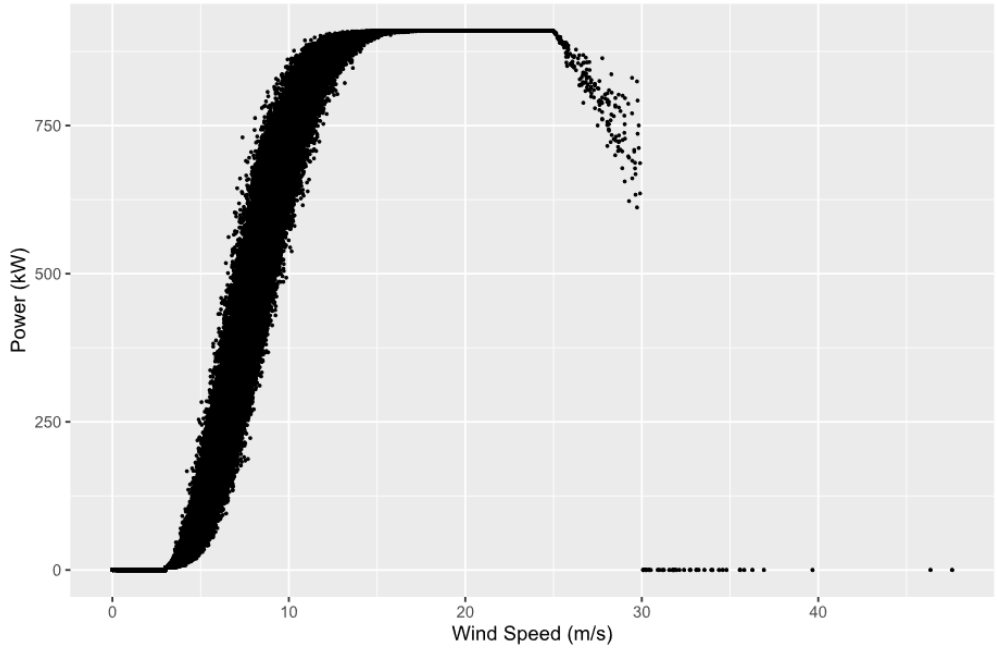

Figure 20: Example of a simulated power curve for Enercon E70-E4

5.2.1.2 Synthetic time series

Exogenous uncertainty in the simulated HRES is incorporated through synthetic time series, which are produced with the anySim R package (Tsoukalas & Kossieris, 2019). AnySim provides models for the simulation of univariate stationary and cyclostationary processes for various distributions, generating synthetic time series with the desired marginal and stochastic properties. In this study, exogenous uncertainty was introduced through the generation of synthetic wind speed and energy demand time series that possess the same statistical properties as the historical data.

5.3 Methodology

This section provides an in-depth analysis of the simulated HRES by specifying the mathematical equations that govern its operation, with a specific focus on the initial two-time steps of the simulation, as the first step slightly deviates from the subsequent ones.

5.3.1 Setting up the simulation

In order to initiate the simulation, it is necessary to set the system's initial conditions and define some key parameters that influence its operation:

1. At the start of the simulation, we consider the reservoir's storage to be approximately 83% of its maximum storage:

$$S_0 = \frac{S_{max}}{1.2} \tag{5.8}$$

2. The power capacity of the pump is calculated as follows:

$$P_{pump}(MW) = \max\left(P_{wind,total}\right) - \min(P_{demand}) \tag{5.9}$$

This assumption is based on the observed data, and specifically on the fact that the maximum energy surpluses occur when renewables produce the most energy and, concurrently, the power demand is the least possible. This instance can occur during late night hours when there is no solar radiation, which is why the latter is not included in equation 5.9.

3. Moreover, a constraint is being set for all time steps concerning the pump's operation:

$$P_{pump}(MW) = \min\left(P_{surpluses}, P_{pump,nominal}\right) \tag{5.10}$$

4. The power capacity of the turbine is calculated as follows:

$$P_{turbine}(MW) = \max(P_{demand}) \tag{5.11}$$

We assume that the maximum energy deficits equal the peak demand of all the generated synthetic time series of energy demand. For reasons of consistency, the energy surpluses and deficits will be expressed in terms of water volume.

5.3.2 Implementation of the simulation.

Firstly, the produced energy from solar radiation and the wind is calculated by extracting the meteorological data from the time series for the given time step (equations 5.1, 5.3, 5.7). The total energy production from renewables is defined as:

$$P_{total}^{(t)} = P_{solar}^{(t)} + P_{wind,total}^{(t)} \tag{5.12}$$

where,

$$P_{wind,total}^{(t)} = P_{wind,large}^{(t)} * N_{large} + P_{wind,small}^{(t)} * N_{small} \tag{5.13}$$

and

$P_{wind,large}^{(t)}$ is the produced energy of a large wind turbine (kW);

N_{large} is the number of large wind turbines used (2);

$P_{wind,small}^{(t)}$ is the produced energy of a small wind turbine (kW)

N_{small} is the number of small wind turbines used (2).

After the total energy production is calculated, it is compared to the power demand of the given time to determine the operation of the pumped water storage:

$$P_{Net}^{(t)} = P_{total}^{(t)} - P_{demand}^{(t)} \tag{5.14}$$

- If $P_{Net}^{(t)} > 0$, there are energy surpluses;
- If $P_{Net}^{(t)} < 0$, there are energy deficits.

To elaborate further, the distinct scenarios of deficits and surpluses are described below.

5.3.3 Pumped water storage operation during energy surpluses

In order to calculate the precipitation and evaporation, we must determine the reservoir's water level through equation 5.5:

$$H^{(t)}(m) = \frac{S_{total}^{(t-1)} + 6{,}280.5}{78{,}793} \tag{5.15}$$

Where:

$S_{total}^{(t-1)}$ is the reservoir's available storage at the beginning of the given time step;

t is an index that acquires values ranging from 1 to the simulation's total steps.

Once the water level is calculated, we utilize equation 5.6 to define the surface area. The surface area will determine the volume of meteorological inflows and outflows. As meteorological inflows, we consider rain:

$$V_{rain}^{(t)}\ (m^3) = A^{(t)}\ (m^2) * Rain^{(t)}\ (mm) \tag{5.16}$$

The rain volume to end up on the reservoir is calculated as follows:

$$V_{rain}^{(t)}(m^3) = \min\left(S_{max} - S_{total}^{(t-1)}, V_{rain}^{(t)}\right) \tag{5.17}$$

As meteorological outflows (losses), we consider evaporation:

$$V_{evap}^{(t)}(m^3) = \max\left(min\left(A^{(t)}(m^2) * Evaporation^{(t)}(mm), S_{total}^{(t-1)} + V_{rain}^{(t)} - V_{dead}\right), 0\right) \tag{5.18}$$

Equation 5.18 outlines that the evaporation cannot be greater than the available water storage. The dead volume is calculated through equation 5.5 for the given depth of 1.2m.

The reservoir's surplus storage is defined as:

$$S_{surplus}^{(t)}(m^3) = S_{max} - \left(S_{total}^{(t-1)} + V_{rain}^{(t)} - V_{evap}^{(t)}\right) \tag{5.19}$$

The volume of the pumped water is set as follows:

$$V_{pump}^{(t)}(m^3) = \min\left(S_{surplus}^{(t)}, \frac{P_{pump}^{(t)} * n_{pump}}{\gamma * H_m} * 1000 * 3600\right) \tag{5.20}$$

where:

γ = 9.81 kN/m^3;

n_{pump} = 0.80 (as per section 5.2);

$Hm = 1.05Dz$, where Dz is the available head (m) (as per section 5.2).

At the end of the time step, the reservoir's available storage is:

$$S_{total}^{(t)}(m^3) = \max\left(S_{total}^{(t-1)} + V_{pump}^{(t)} + V_{rain}^{(t)} - V_{evap}^{(t)}, V_{dead}\right) \tag{5.21}$$

5.3.4 Pumped water storage operation during energy deficits

This section outlines the operation of the system during energy deficits. The methodology is identical to the one described in section 5.3.3. Therefore, to define the reservoir's water level, surface area, and meteorological inflows and outflows, we utilize equations 5.5, 5.6, 5.16, 5.17 and 5.18. In order to satisfy energy demand, the available head is utilized to produce hydro energy through the turbines. The power of the turbine at the given time is defined as follows:

$$P_{prod}^{t}(MW) = \min\left(Deficits^{(t)}, P_{turbine}\right) \tag{5.22}$$

We can now calculate the volume of the water required to produce the power mentioned above:

$$V_{prod}^{(t)}(m^3) = \min\left(\max\left(S_{total}^{(t-1)} + V_{rain}^{(t)} - V_{evap}^{(t)} - V_{dead}, 0\right), \frac{P_{prod}^{(t)} * 1000}{n_{turb} * \gamma * H_n} * 3600\right) \tag{5.23}$$

where:

γ = 9.81 kN/m^3;

n_{turb} = 0.85 (as per section 5.2);

$Hn = 0.95 * Dz$, where Dz is the available head (m) (as per section 5.2);

The surplus storage and total storage at the end of the first step are set as follows:

$$S_{surplus}^{(t)}(m^3) = S_{max} - \left(S_{total}^{(t-1)} - V_{prod}^{(t)} + V_{rain}^{(t)} - V_{evap}^{(t)}\right) \tag{5.24}$$

$$S_{total}^{(t)}(m^3) = \max\left(S_{total}^{(t-1)} - V_{prod}^{(t)} + V_{rain}^{(t)} - V_{evap}^{(t)}, V_{dead}\right) \tag{5.25}$$

5.4 Evaluation of the system

The techno-economic evaluation is a crucial step in the system's development and implementation, as it helps assess the proposed solution's feasibility and viability. The process involves systematically examining the design's technical, economic, and financial aspects.

In order to assess the system's feasibility and cost-effectiveness, we define essential economic metrics (Table 3):

Table 3: Indicative cost of HRES' components

Component	Cost	
Excavation	6	€/m^3
Waterproofing membrane	1.5	€/m^2
Penstock	25	€/m
Wind power	1,200,000	€/MW produced
Solar power	1,100,000	€/MW installed
Wind turbine maintenance (annual)	0.015	€/kWh produced
Photovoltaics maintenance (annual)	1%	of the initial cost

To calculate the cost of the pumped water storage's turbine and pump, we use the following formula proposed by Aggidis *et al.* (2010):

$$C = C_0 I^{\alpha} h^{\beta} \tag{5.26}$$

where:

C_0 = 14,400 €;

α = 0.56;

β = -0.112;

I is the power capacity (kW);

h is the gross head (m).

All the components costs mentioned will be expressed in terms of annual installments according to the following formula:

$$A = C \frac{i(1+i)^n}{(1+i)^n - 1} \tag{5.27}$$

where:

n is the years;

C is the total investment cost;

i is the interest rate.

For the mechanological equipment, we consider total depreciation in 10 years, whereas, for the cost of all the works concerning the reservoir, we consider total depreciation in 20 years.

Another crucial metric for the system's evaluation is its reliability. The reliability of an HRES can concern both energy deficits and frequency aspects. The former metric refers to how much of the total energy demand the HRES can cover, while the latter refers to the number of times the HRES can cover that demand in a given time horizon. Both of the aforementioned metrics are expressed in economic terms.

For the system's economic assessment:

- Every MW of produced energy brings 300€ of profit to the system;
- Every MW of unfulfilled energy demand causes 350€ losses to the system.

We consider a logarithmic curve for the frequency facet of reliability to simulate the imposed penalty (Figure 21). This curve can be tuned depending on the system's desired level of reliability.

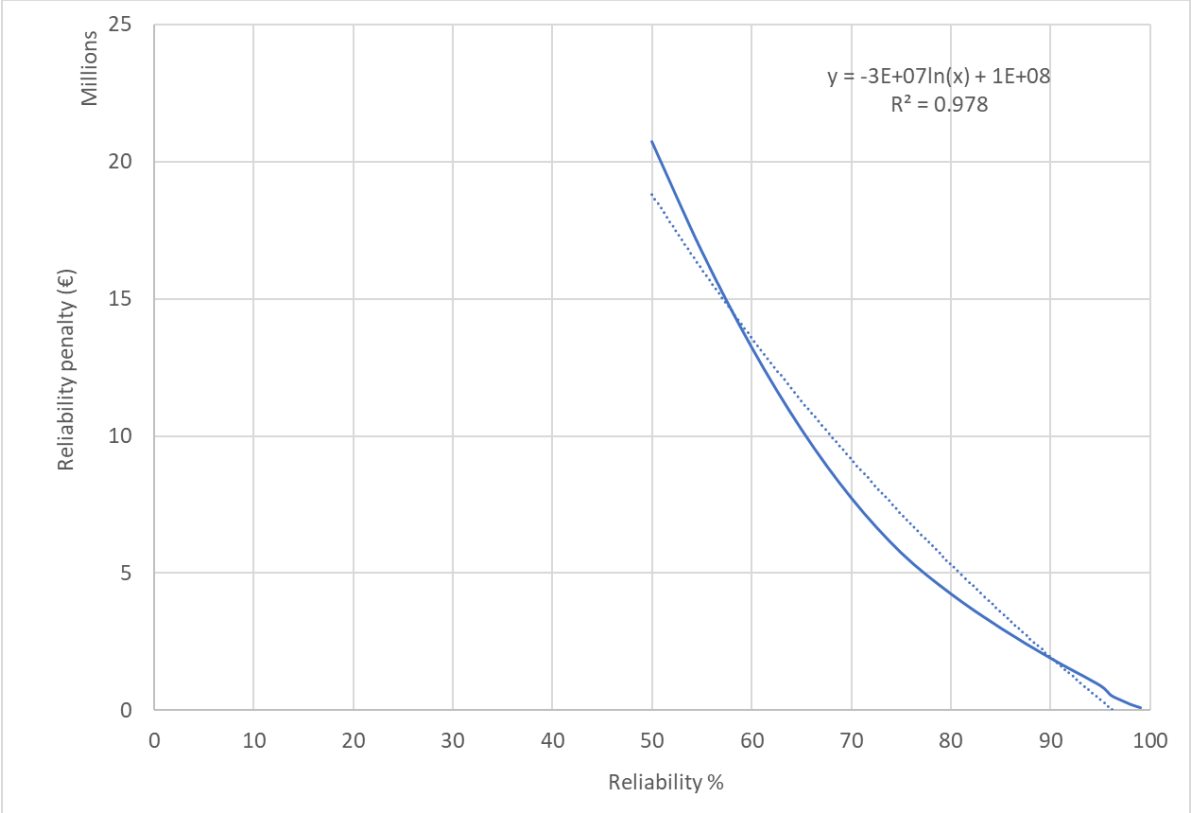

Figure 21: Reliability penalty evolution

It is important to consider that all of the aforementioned evaluation metrics are dependent on random variables, thus they are stochastic by default.

6. Optimization of the model in the Rstudio environment

This section outlines the methodology of the system's optimization, which was performed in the Rstudio programming environment.

6.1 Input data

As a first step, time series of the prerequisite data for implementation of the simulation (wind speed, solar irradiation, energy demand, evaporation, precipitation) are imported from MS Excel spreadsheets into Rstudio as data frames (Figure 22). The time series provide 20 years of data in an hourly time step (175,200 steps total).

```
solar_data<-read_excel("Solar_data.xlsx")
sun_data<-data.frame(solar_data)


wind_data<-read_excel("Wind_synthetic.xlsx")
w_d<-data.frame(wind_data)


Precip<-read_excel("Precipitation.xlsx")
Precip<-data.frame(Precip)

Evap<-read_excel("Evaporation.xlsx")
Evap<-data.frame(Evap)

demand<-read_excel("Demand_energy_teliko1.xlsx")
demand<-data.frame(demand)
```

Figure 22: Importing the time series data into Rstudio

Other input data included in the simulation are outlined in section 5.2.

6.2 Functions used

All the equations defined in chapter 5 are included in the Rstudio environment as functions. Figure 23 portrays the analytical formula of the produced power of a wind turbine that implements the soft cut-out strategy (equations 5.3 & 5.7).

```
analytical_wind_speed<-function(v_wind,pmin,pmax,a,b,vmin,vmax,steps,angle){
  p<-rep(0,steps)
  for (i in 1:steps){

  if(v_wind[i]>vmin && v_wind[i]<vmax){
    p[i]=pmin+(1-(1-((v_wind[i]-vmin)/(vmax-vmin))^a[i])^b[i])*(pmax-pmin)
  }else if (v_wind[i]>vmax && v_wind[i]<=30 ){
    p[i]=pmax-angle[i]*(v_wind[i]-vmax)
  }else {
    p[i]=0
  }

  }
  return(p)
}
```

Figure 23: Analytical power equation with soft cut-out strategy in Rstudio

The incorporation of uncertainty for the variables a, b, and the slope of the linear power reduction in the high-speed region is presented in Figure 24, where "simsteps" equals the total steps of the simulation.

```
a<-rnorm(simsteps,mean=2.25,sd=0.15)
b<-rnorm(simsteps,mean=20,sd=0.4)
angle_L<-rnorm(simsteps,mean=150,sd=15)
angle_S<-rnorm(simsteps,mean=45,sd=10)
```

Figure 24: Representation of uncertainty in wind power production

The wind speed reduction at the small wind turbine's hub due to interaction is shown in Figure 25 (equation 5.4).

```
wind_speed_reduction_due_to_interaction<-function(v_wind,a,k,Distance,D_turb_large,steps){
  v_wind_red<-rep(0,steps)
  for (i in 1:steps){
  v_wind_red[i]<-v_wind[i]*(1-2*a/((1+2*k*Distance/D_turb_large)^2))
  }
  return(v_wind_red)
}
```

Figure 25: Representation of wind speed reduction due to wind turbine interaction

The code for the reservoir inflows and outflows, as described in section 5.3, is shown in Figure 26 & Figure 27.

```
H_reserv[1]<-(S0+6280.5)/78793
A_reservoir_m2[1]<- 763.89*H_reserv[1]+74978
Rain[1]<-Precip[1]/1000*A_reservoir_m2[1]
Evaporation[1]<- min(S0+Rain[1],Evap[1]/1000*A_reservoir_m2[1])

for (i in 1:steps){
  P_pump[i]<-min(surplusses[i],max_pump_MW)
}

if(deficits[1]<0){
V_prod[1]<-min(S0+Rain[1]-Evaporation[1],-deficits[1]/nturb/9.81/Hn*1000*3600)
V_pump[1]=0
Surplus_storage[1]<-Smax-(S0-V_prod[1])
}else{
  V_prod[1]<-0
  Surplus_storage[1]<-Smax-(S0-V_prod[1]+Rain[1]-Evaporation[1])
  V_pump[1]<-min(Surplus_storage[1],P_pump[1]*npump/9.81/Hm*1000*3600)
}


V_equilibr[1]<-max(S0+V_pump[1]-V_prod[1]+Rain[1]-Evaporation[1],V_dead)
```

Figure 26: First step of the reservoir's hydrological simulation

```
for (i in 2:steps){

  if(deficits[i]<0){
    H_reserv[i]<-(V_equilibr[i-1]+6280.5)/78793
    A_reservoir_m2[i]<- 763.89*H_reserv[i] + 74978
    Rain[i]<-min(Smax-V_equilibr[i-1],Precip[i]/1000*A_reservoir_m2[i])
    Evaporation[i]<-min(V_equilibr[i-1]+Rain[i],Evap[i]/1000*A_reservoir_m2[i])
    V_prod[i]<-min(max(V_equilibr[i-1]+Rain[i]-Evaporation[i]-V_dead,0),-deficits[i]/nturb/9.81/Hn*1000*3600)
    V_pump[i]<-0
    Surplus_storage[i]<-Smax-(V_equilibr[i-1]-V_prod[i]+Rain[i]-Evaporation[i])
    V_equilibr[i]<-max(V_equilibr[i-1]+V_pump[i]-V_prod[i] + Rain[i] - Evaporation[i],0)
   }else {
     H_reserv[i]<-(V_equilibr[i-1]+6280.5)/78793
     A_reservoir_m2[i]<- 763.89*H_reserv[i] + 74978
     V_prod[i]<-0
      Rain[i]<-min(Smax-V_equilibr[i-1],Precip[i]/1000*A_reservoir_m2[i])
      Evaporation[i]<-min(V_equilibr[i-1]+Rain[i],Evap[i]/1000*A_reservoir_m2[i])
      Surplus_storage[i]<-Smax-(V_equilibr[i-1]-V_prod[i]+Rain[i]-Evaporation[i])
      V_pump[i]<-min(Surplus_storage[i],P_pump[i]*npump/9.81/Hm*1000*3600)
      V_equilibr[i]<-max(V_equilibr[i-1]+V_pump[i]-V_prod[i]+Rain[i]-Evaporation[i],0)
    }
}
```

Figure 27: Subsequent steps of the reservoir's hydrological simulation

Lastly, Figure 28 depicts the code used for the reservoir's hydrological simulation for j individual scenarios produced by the generated synthetic time series.

```
if(deficits[i,j]<0){
  H_reserv[i,j]<-(V_equilibr[i-1,j]+6280.5)/78793
  A_reservoir_m2[i,j]<- 763.89*H_reserv[i,j] + 74978
  Rain[i,j]<-min(Smax-V_equilibr[i-1,j],Precip[i,j]/1000*A_reservoir_m2[i,j])
  Evaporation[i,j]<-min(V_equilibr[i-1,j]+Rain[i,j],Evap[i,j]/1000*A_reservoir_m2[i,j])
  V_prod[i,j]<-min(max(V_equilibr[i-1,j]+Rain[i,j]-Evaporation[i,j]-V_dead,0),-deficits[i,j]/nturb/9.81/Hn*1000*3600)
  V_pump[i,j]<-0
  Surplus_storage[i,j]<-Smax-(V_equilibr[i-1,j]-V_prod[i,j]+Rain[i,j]-Evaporation[i,j])
  V_equilibr[i,j]<-max(V_equilibr[i-1,j]+V_pump[i,j]-V_prod[i,j] + Rain[i,j] - Evaporation[i,j],0)
 }else {
   H_reserv[i,j]<-(V_equilibr[i-1,j]+6280.5)/78793
   A_reservoir_m2[i,j]<- 763.89*H_reserv[i,j] + 74978
   V_prod[i,j]<-0
    Rain[i,j]<-min(Smax-V_equilibr[i-1,j],Precip[i,j]/1000*A_reservoir_m2[i,j])
    Evaporation[i,j]<-min(V_equilibr[i-1,j]+Rain[i,j],Evap[i,j]/1000*A_reservoir_m2[i,j])
    Surplus_storage[i,j]<-Smax-(V_equilibr[i-1,j]-V_prod[i,j]+Rain[i,j]-Evaporation[i,j])
    V_pump[i,j]<-min(Surplus_storage[i,j],P_pump[i,j]*npump/9.81/Hm*1000*3600)
    V_equilibr[i,j]<-max(V_equilibr[i-1,j]+V_pump[i,j]-V_prod[i,j]+Rain[i,j]-Evaporation[i,j],0)
```

Figure 28: Subsequent steps of the reservoir's hydrological equilibrium for j simulations

6.3 Problem setting

The optimization of the hybrid renewable energy system is formulated as a single-objective optimization problem. The flow chart describing the system's operation and optimization is presented in Figure 29. The system's operation has been analyzed in section 5.3. The primary problem variables are the reservoir height and the number of PV modules. Identifying the optimum set of these variables requires defining an objective function representing the minimization of operating costs and appropriately annualized installation costs. The system's reliability has also been expressed in economic terms in section 5.4. Thus, by optimizing the system's annual profits, we also achieve high reliability in covering energy needs.

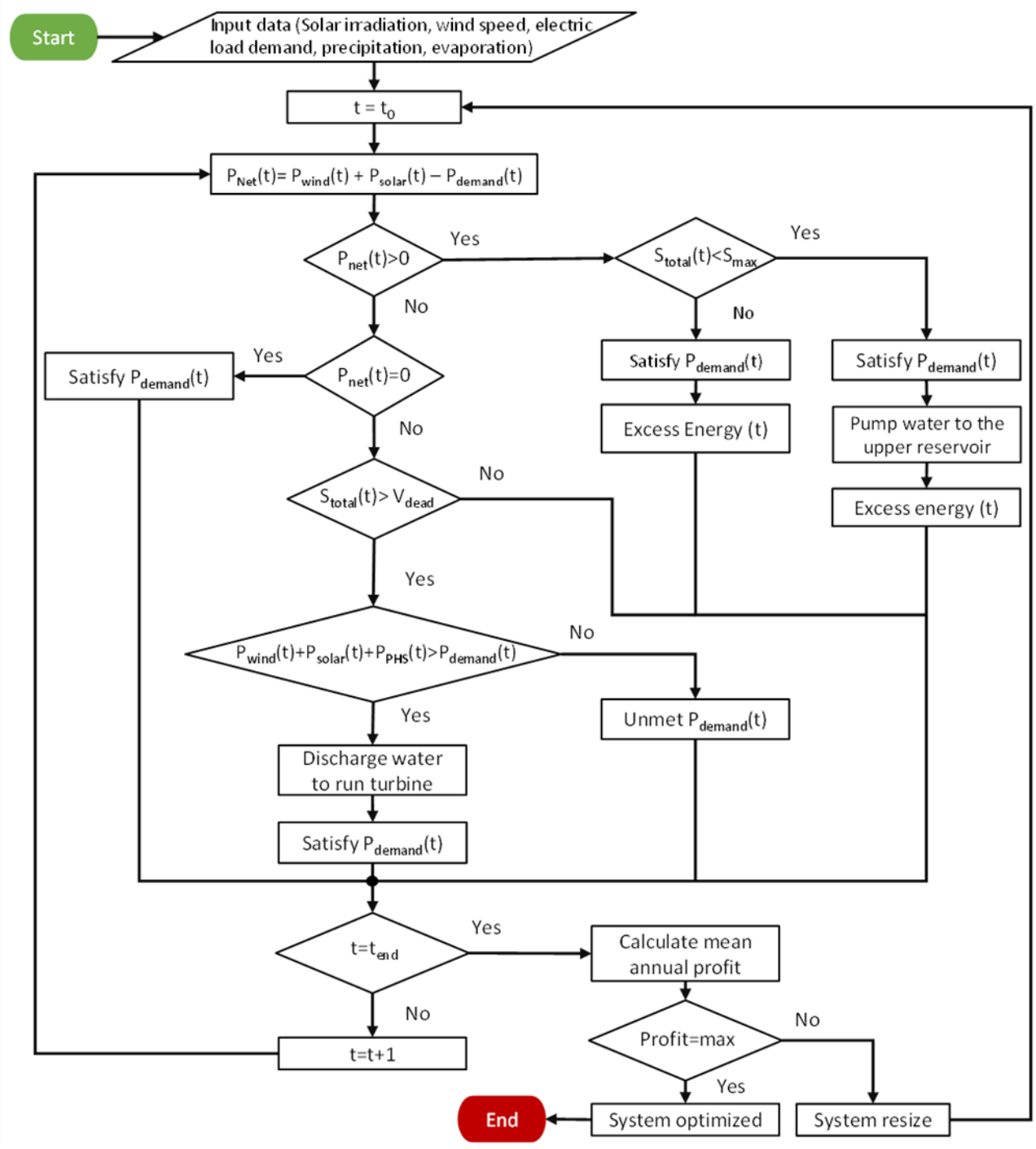

Figure 29: HRES optimization method flowchart

6.4 Optimization method

For the system's optimization, we utilize the evolutionary annealing-simplex algorithm (Efstratiadis & Koutsogiannis, 2002) R-package "EAS". EAS is a probabilistic heuristic global optimization technique, combining the robustness of simulated annealing in rough response surface with the efficiency of hill-climbing methods in convex areas. The input control variables are the reservoir depth and the number of PV modules, while the objective function aims to maximize the system's annual profit. To perform the optimization, we define the interior lower and upper bounds of the control variables as a vector and the maximum number of function evaluations. For our case study, we set the lower bounds to be the vector ($h_{reservoir}$, PV) = (1,100) and the upper bounds as the vector (10,5000) to ensure that the project remains at a feasible scale from a technical perspective. The number of evaluations was set to 100.

7. Results of investigated scenarios

This chapter aims to present the results of the simulated scenarios. First, we analyze the HRES sizing scenarios as proposed in the study of Katsaprakakis & Voumvoulakis (2018), which was the motivation of this thesis. These are considered to be the baseline scenarios. Following this, we present our proposed optimized baseline scenario based on the assumptions and methodology of chapter 5. We then present the results of 100 stochastic-generated optimized scenarios.

7.1 Baseline scenarios

Katsaprakakis & Voumvoulakis suggested that the reservoir's capacity would be 1,100,000 m^3, then presented three distinct scenarios on the use of renewables. We further examine these scenarios to determine the system's overall reliability and economic feasibility:

- The first scenario includes 3 wind turbines of 2.3 MW nominal power each (6.9 MW of wind park) along with 2 MW of PV modules;
- The second scenario includes 4 wind turbines of 2.3 MW nominal power each (9.2 MW of wind park) along with 0.5 MW of PV modules;
- The third scenario includes 5 wind turbines of 2.3 MW nominal power each (11.5 MW of wind park) and no PV modules.

The scenarios' key characteristics and simulation results are summarized in Table 4:

Table 4: Summary of the key findings for the simulated scenarios

	Scenario 1	Scenario 2	Scenario 3
Installed Wind Power (MW)	6.90	9.20	11.50
Installed Solar Power (MW)	2	0.50	0
Mean annual energy from renewables (GWh)	29.25	35.10	42.75
Mean annual energy from PHS (GWh)	4.90	4.98	4.88
Reliability %	99.30	99.40	99.60
Mean annual profit (€)	911,000	760,333	546,700

All these solutions guarantee sufficient energy production, given that the expected annual electricity consumption for 2020 was 18,86 GWh (Katsaprakakis & Voumvoulakis), and high reliability. The simulated system results also confirm the conclusion of their study that the first scenario is the most favorable from an economic perspective. However, all of the aforementioned scenarios suggest excavating a 1,100,000 m^3 reservoir. Many technical and functional issues arise with the introduction of such large-scale works. Thus, it is necessary for us to propose a baseline scenario of a smaller-scale project while still maintaining high-reliability levels.

7.2 Proposed baseline scenario

The key elements of the baseline scenario proposed in this thesis are outlined in chapter 5. This scenario has been optimized in R-studio to maximize the mean annual profit while changing the reservoir's storage and number of PV modules. Its key results are shown in Table 5. The installed wind power corresponds to 4 wind turbines, 2 of 2.3 MW nominal power each and 2 of 0.9 MW nominal power each.

Table 5: Key results of the proposed optimized baseline scenario

Optimized proposed baseline scenario	
Reservoir Volume (m^3)	315,195
Installed Wind Power (MW)	6.40
Installed Solar Power (MW)	1.09
Mean annual energy from renewables (GWh)	24.98
Mean annual energy from PHS (GWh)	4.69
Reliability %	94.76
Mean annual profit (€)	789,131
Capacity Factor	
Photovoltaics	0.207
Small Wind turbines	0.304
Large Wind turbines	0.424
Pumped Water Storage	0.108

Comparing the results of our proposed optimized baseline scenario to the ones of section 7.1, we notice that this system, with a reservoir capacity equal to less than a third of the one initially proposed, continues to exhibit high reliability levels while maintaining the mean annual profit at the same level. The capacity factor for each sub-system has also been calculated. The low value of the pumped water storage's capacity factor indicates that it is primarily used to cover the energy hourly demand peaks. Figure 30 presents the fluctuation of the reservoir's storage throughout the simulation.

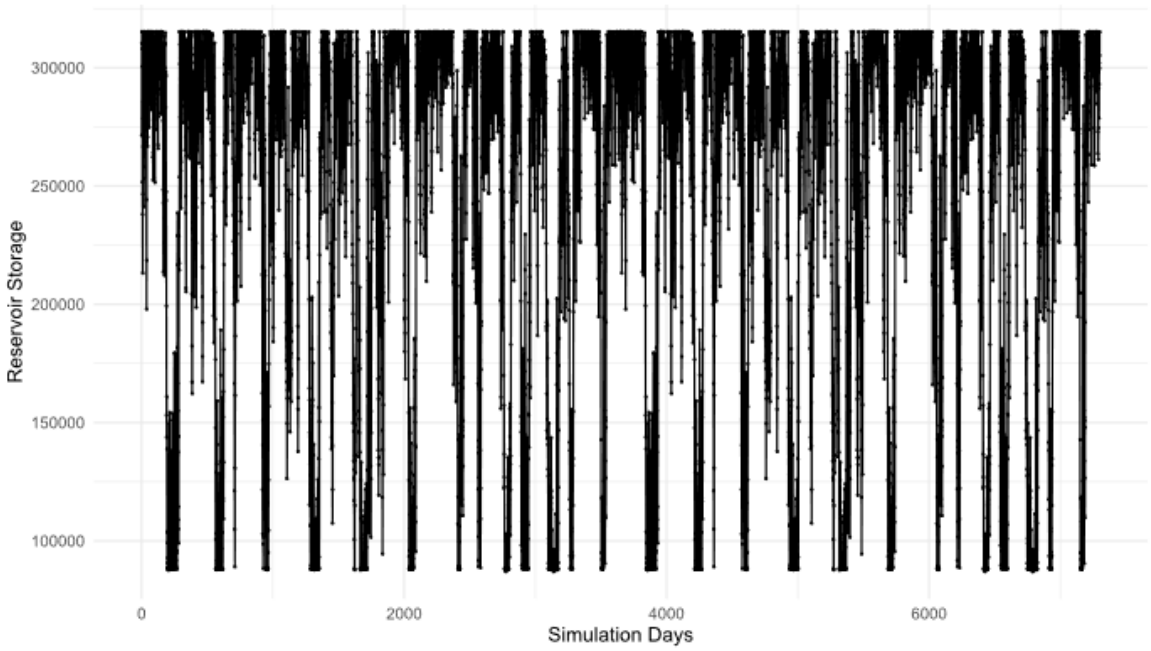

Figure 30: Reservoir storage fluctuation

7.3 Uncertainty scenarios

In this section, we present the results of the optimized system described in section 7.2 under uncertainty. Specifically, 100 scenarios were optimized using the synthetic generated time-series for wind speed and power demand. The statistical properties of HRES' key metric, as well as the 10%, 50%, and 90% quantiles are summarized in Table 6. The installed solar modules correspond to almost 1.7 MW of power for all the investigated scenarios. New metrics are being introduced into the results, namely the number of PV modules and the mean annual deficit hours, in order to provide a better understanding of the system's operation for the different scenarios.

Following the presented results, we make the following observations:

- The HRES continues to exhibit high levels of reliability among the majority of the optimized scenarios;
- The scenarios with larger reservoir volume exhibit higher levels of reliability, and, therefore, higher mean annual profit.
- The pumped hydro storage has a relatively low capacity factor in all scenarios, indicating that it is primarily used to cover the hourly energy peaks.

After comparing the quantiles of the simulated scenarios, it is understood that uncertainty incorporation leads to significant variance in the reservoir volume, the mean annual energy from renewables and the system's reliability. Another important observation is the fluctuation of the capacity factor values for the wind turbines among the scenarios. This highlights the significant level of uncertainty that wind speed and power conversion processes introduce in wind energy production.

Table 6: HRES key metrics from the 100 optimized scenarios

	Mean	Standard deviation	Coefficient of variation	10% Quantile	50% Quantile	90% Quantile
Reservoir Volume (m^3)	329,882	53,370	0.16	400,282	323,278	274,583
Installed PV Modules	4981	74.4	0.015	5000	5000	4981
Mean annual energy from renewables (GWh)	24.24	1.90	0.08	26.78	24.43	21.86
Mean annual energy from PHS (GWh)	4.93	0.19	0.04	5.16	4.95	4.69
Mean annual energy deficit time (hours)	447	131	0.29	618	431	288
Reliability %	94.89	1.50	0.02	96.75	95.11	92.98
Mean annual profit (€)	640,234	255,052	0.40	959,029	669,924	315,269
Small wind turbine capacity factor	0.292	0.033	0.114	0.339	0.295	0.252
Large wind turbine capacity factor	0.411	0.034	0.084	0.459	0.414	0.367
Pumped water storage capacity factor	0.089	0.006	0.096	0.096	0.090	0.082

Moreover, the normal and log-normal distributions are fit to the optimal values of the reservoir's occupied height and mean annual profit. This is achieved by using the *"fitdistrplus"* R package, which provides functions for fitting univariate distributions to different types of data (continuous censored or non-censored data and discrete data), allowing different estimation methods. For our data, we choose the moment-matching estimation method, which involves finding the values of the model parameters that make the data's sample moments equal to the model's corresponding population moments. Figure 31 & Figure 32 depict the density functions, while Figure 33 & Figure 34 present the cumulative density functions.

Lastly, a Gaussian copula is fitted to quantify the predictive uncertainty of the mean annual profit and the reservoir's occupied height with a coefficient of determination (R^2) equal to -0.75, as shown in Figure 35. Copula theory enables the construction of multivariate joint distributions with arbitrary marginals. A copula can be utilized by both an engineer and a potential investor as a decision support tool for system planning under uncertainty. In our case, we provide a correlation between the mean annual profit and the reservoir's occupied height with an 80% confidence level.

This way, for a given reservoir height, we can predict possible margins of the mean annual profit, and vice versa.

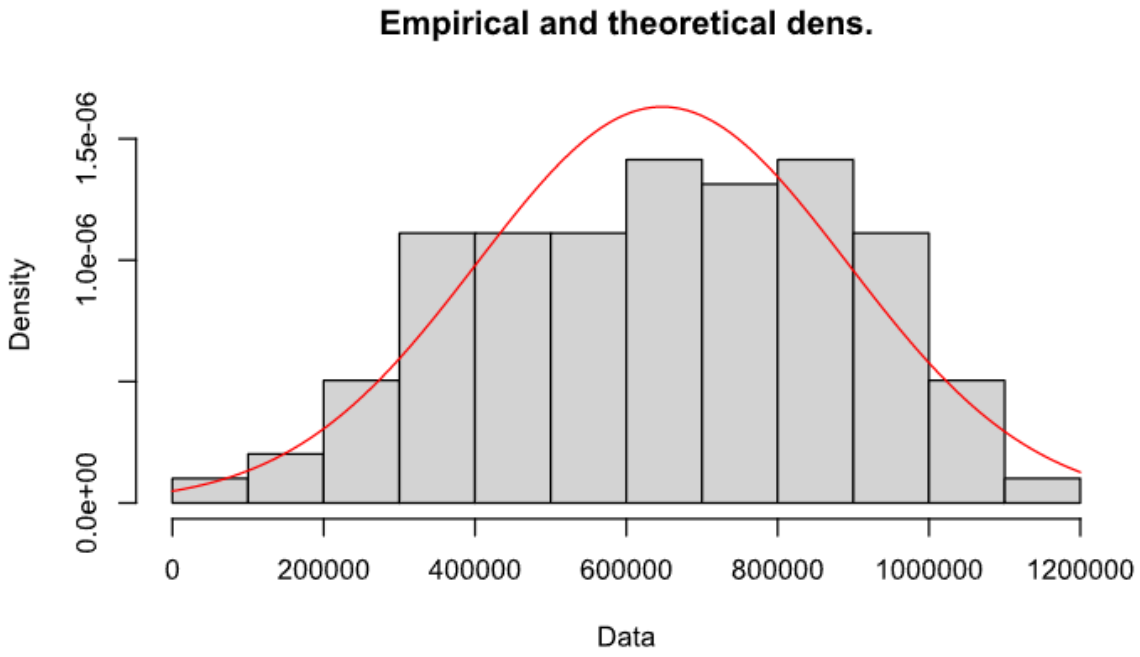

Figure 31: Fitting of Normal distribution to the set of optimized mean annual profit values

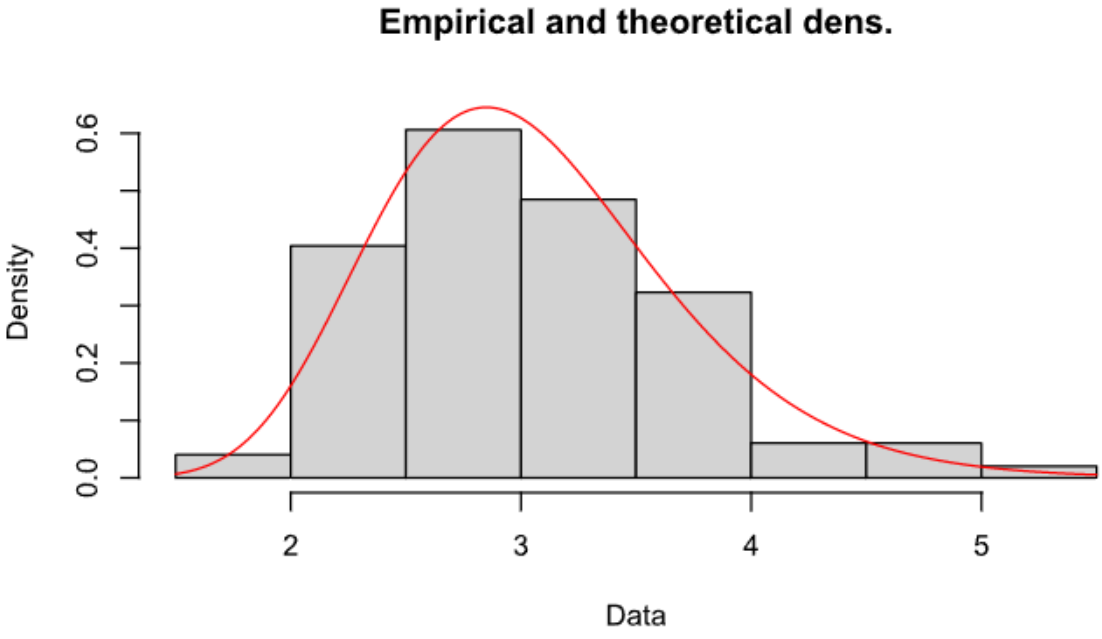

Figure 32: Fitting of Log-Normal distribution to the set of optimized reservoir's occupied height values

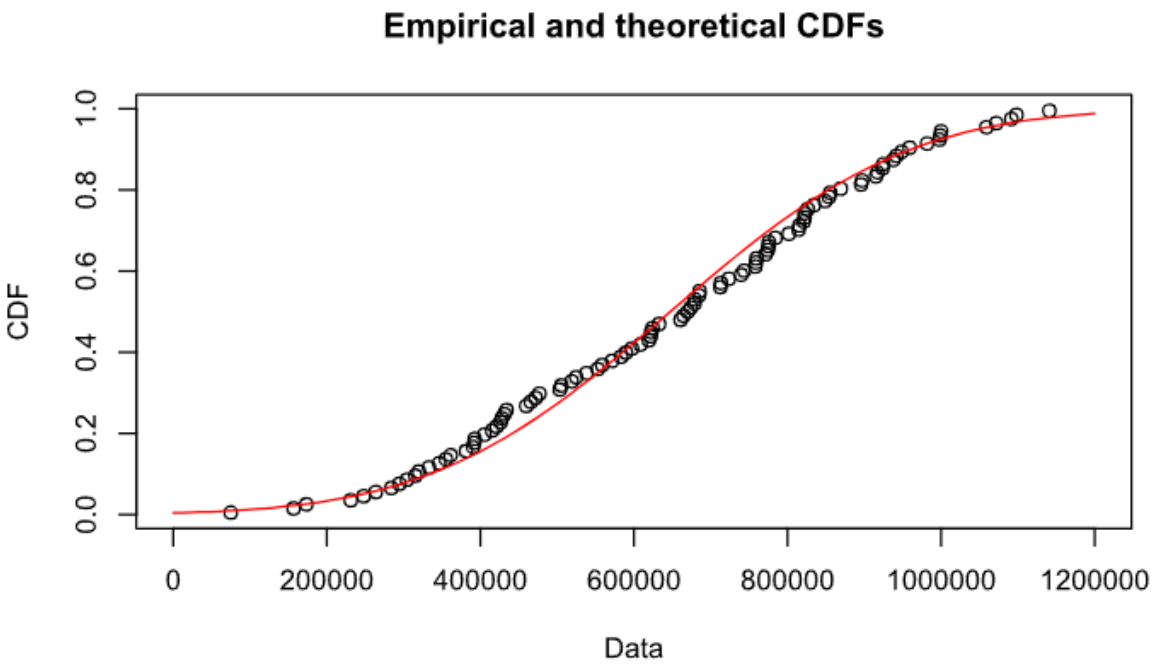

Figure 33: Fitting of the optimized mean annual profit values to the cumulative density function

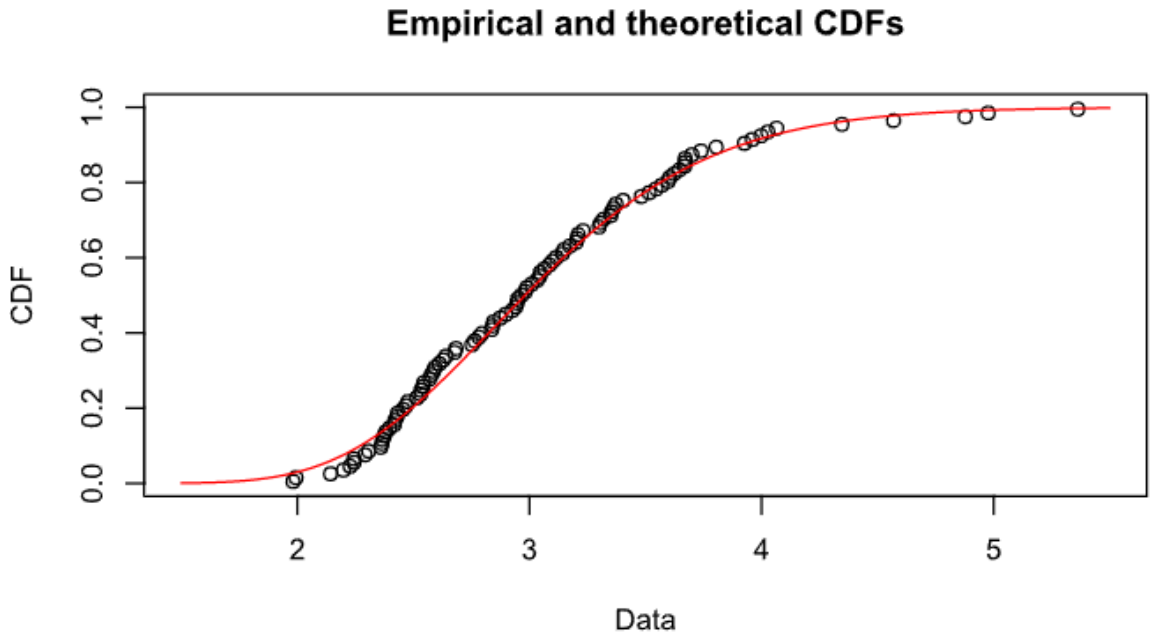

Figure 34: Fitting of the optimized reservoir's occupied height values to the cumulative density function

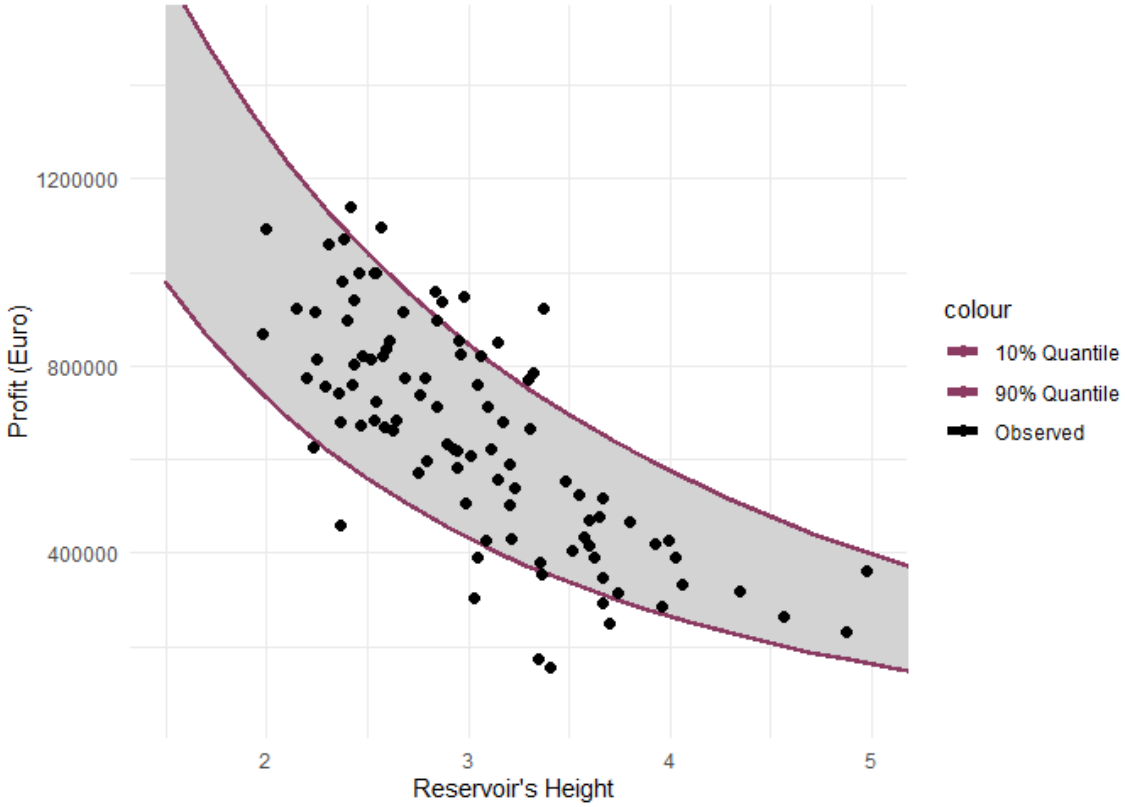

Figure 35: Fitting of Gaussian copula to mean annual profit and reservoir occupied height

8. Conclusions

8.1 Thesis conclusions

The purpose of this thesis was to investigate the impact of uncertainty in the planning of a hybrid renewable energy system. Multiple facets of uncertainty (exogenous and endogenous) were addressed in order to provide a comprehensive analysis.

Firstly, we provided an analysis of the components of an HRES and the interdependencies of its sub-systems. Potential issues of uncertainty that must be considered during both the planning and operation phases are also presented. These can either be of exogenous nature (i.e., meteorological processes and energy demand) or of endogenous nature (i.e., wind power production).

Since the analysis of this thesis was built upon a proposed HRES in the island of Sifnos, including a seawater pumped storage, we evaluate the proposed scenarios while also addressing technical challenges concerning the use of seawater. The evaluation procedure is undertaken by configuring an HRES operation model for an hourly-step analysis to simulate the aforementioned scenarios, outlining the reservoir's inflows and outflows, as well as its interdependency with renewable energy production. We then suggest our own deterministic approach on the system's design.

Following this, we presented a single objective optimization problem of our proposed HRES based on two control variables: the reservoir's height and the number of PV modules. The system was optimized under uncertainty based on economic and reliability criteria, which are briefly analyzed. This was achieved through the use of an evolutionary annealing-simplex algorithm.

After comparing our deterministic system approach to the proposed baseline scenarios, we conclude that our proposed system can exhibit high levels of reliability, even though it is of a much smaller scale than the one initially proposed. We then proceed to conduct a more realistic analysis of the system's operation by incorporating uncertainty in 100 stochastic generated scenarios. The optimization results revealed that incorporating uncertainty in HRES leads to significant variation in the annual profit, the energy produced and its reliability. Lastly, we fit our key metrics to statistic distributions to provide a better understanding of the simulations' results and we use a Gaussian copula to quantify the predictive uncertainty of the mean annual profit and reservoir height values from the 100 optimized scenarios.

8.2 Future research perspectives

While the proposed system was investigated and optimized under uncertainty, we have identified several issues for future research regarding the planning and operation of the HRES. These can be subdivided in categories.

1. Design issues:
    - The installation of floating photovoltaics on the surface of the reservoir could significantly reduce evaporation losses.

2. Issues related to the HRES operation model:
    - In order to provide a more realistic approach on the operation of the pumped water storage, it is beneficial to consider that the turbine and pump do not operate at a constant efficiency rate.
    - The effect of sea water on the equipment needs to be further investigated throughout the system's operation. This way, the hydraulic processes and calculations can be conducted in a more accurate manner.

3. Further uncertainty issues. This study mainly analyzed uncertainties in wind power and energy demand, thus other facets of uncertainty need to be further examined, such as:
    - The uncertainty in solar irradiation (physical process);
    - The uncertainty in solar power production (internal process);
    - The uncertainty in the market of energy (dependent on socio-economic parameters).

4. Other research perspectives:
    - In order to achieve high reliability over the lifespan of an HRES (approximately 20 years), it is expected that there will be excess energy left unexploited when the upper reservoir is full. Thus, it is encouraged to investigate whether that excess energy can be utilized.

References

Abdel-Aal, R. E. (2008). Univariate modeling and forecasting of monthly energy demand time series using abductive and neural networks. Computers and Industrial Engineering, 54(4), 903e917. https://doi.org/10.1016/j.cie.2007.10.020.

Aggidis GA, Luchinskaya E, Rothschild R, Howard DC. The costs of small-scale hydro power production: Impact on the development of existing potential. Renew Energy 2010;35:2632–8. https://doi.org/10.1016/j.renene.2010.04.008.

Ali, S.; Jang, C.-M. Optimum Design of Hybrid Renewable Energy System for Sustainable Energy Supply to a Remote Island. Sustainability 2020, 12, 1280. https://doi.org/10.3390/su12031280

Andrew Blakers et al 2021 Prog. Energy 3 022003

Astolfi, D., Castellani, F., Lombardi, A., & Terzi, L. (2018). About the extension of wind turbine power curve in the high wind region. Journal of Solar Energy Engineering. doi:10.1115/1.4041156

Bajpai, P., & Dash, V. (2012). Hybrid renewable energy systems for power generation in stand-alone applications: A review. Renewable and Sustainable Energy Reviews, 16(5), 2926–2939. doi:10.1016/j.rser.2012.02.009

Bashahu, M., and J. C. Nsabimana. "Statistical analysis of sunshine duration measurements in Burundi using beta distributions." World Conference on Physics and Sustainable Development Durban Poster No102244, South Africa. 2005.

Cabeza, L. F., Palacios, A., Serrano, S., Ürge-Vorsatz, D., & Barreneche, C. (2018). Comparison of past projections of global and regional primary and final energy consumption with historical data. Renewable and Sustainable Energy Reviews, 82, 681–688. doi:10.1016/j.rser.2017.09.073

Caralis, G., Rados, K., & Zervos, A. (2010). On the market of wind with hydro-pumped storage systems in autonomous Greek islands. Renewable and Sustainable Energy Reviews, 14(8), 2221–2226. doi:10.1016/j.rser.2010.02.008

Carta, J. A., Ramírez, P., & Velázquez, S. (2009). A review of wind speed probability distributions used in wind energy analysis. Renewable and Sustainable Energy Reviews, 13(5), 933–955. doi:10.1016/j.rser.2008.05.005

Castellani, F., Natili, F., Astolfi, D., & Cianetti, F. (2019). Mechanical behaviour of wind turbines operating above design conditions. Procedia Structural Integrity, 24, 495–509. doi:10.1016/j.prostr.2020.02.045

Das, P., Das, B. K., Mustafi, N. N., & Sakir, M. T. (2021). A review on pump-hydro storage for renewable and hybrid energy systems applications. Energy Storage, 3(4). doi:10.1002/est2.223

Dimitris Al Katsaprakakis, Manolis Voumvoulakis, A hybrid power plant towards 100% energy autonomy for the island of Sifnos, Greece. Perspectives created from energy cooperatives, Energy, Volume 161, 2018, Pages 680-698, ISSN 0360-5442, https://doi.org/10.1016/j.energy.2018.07.198.

Efstratiadis, A. & Koutsoyiannis, D. (2002). An evolutionary annealing-simplex algorithm for global optimization of water resource systems, Proceedings of the Fifth International Conference on Hydroinformatics, Cardiff, UK, 1423–1428, International Water Association.

Eltamaly, A. M., Alotaibi, M. A., Alolah, A. I., & Ahmed, M. A. (2021). IoT-Based Hybrid Renewable Energy System for Smart Campus. Sustainability, 13(15), 8555. doi:10.3390/su13158555

Faccio, M., Gamberi, M., Bortolini, M. et al. State-of-art review of the optimization methods to design the configuration of hybrid renewable energy systems (HRESs). Front. Energy 12, 591–622 (2018). https://doi.org/10.1007/s11708-018-0567-x

Francis, Roger, and Stan Hebdon. "The Selection of Stainless Steels for Seawater Pumps." Paper presented at the CORROSION 2015, Dallas, Texas, March 2015.

G.K. Sakki, I. Tsoukalas, P. Kossieris, C. Makropoulos, A. Efstratiadis, Stochastic simulation-optimization framework for the design and assessment of renewable energy systems under uncertainty, Renewable and Sustainable Energy Reviews, Volume 168, 2022, 112886, ISSN 1364-0321, https://doi.org/10.1016/j.rser.2022.112886.

Georgios Tsekouras, Demetris Koutsoyiannis, Stochastic analysis and simulation of hydrometeorological processes associated with wind and solar energy, Renewable Energy, Volume 63, 2014, Pages 624-633, ISSN 0960-1481, https://doi.org/10.1016/j.renene.2013.10.018.

Hydrognomon: A Database System for the Management of Hydrometeorological Stations and Time Series. Hydrological Time Series Analysis and Processing Software Application. 2012. https://hydrognomon.openmeteo.org/

Islam, M. A., Che, H. S., Hasanuzzaman, M., & Rahim, N. A. (2020). Energy demand forecasting. Energy for Sustainable Development, 105–123. doi:10.1016/b978-0-12-814645-3.00005-5

J.J. Ding and J. S. Buckeridge, “Design considerations for a sustainable hybrid energy system” in IPENZ Transactions, Vol. 27, No. 1/EMCh (2000). Available from www.ipenz.org.nz/ipenz/publications/transactions/Transactions2000/TransEMCh00/1ding1.pdf

Jacob T. Pumped storage in Switzerland—an outlook beyond 2000, Stucky Consulting Engineers Ltd., Post Box 1000 Lausanne 6, Switzerland, The Economist 2011-03-03. Retrieved 2014-02-18; 2014.

Jelavic, Mate, et al. "Wind turbine control beyond the cut-out wind speed." Annual Conference and Exhibition of European Wind Energy Association (EWEA2013). 2013.

K. Warren et al., "Managing uncertainty in electricity generation and demand forecasting," in IBM Journal of Research and Development, vol. 60, no. 1, pp. 8:1-8:13, Jan.-Feb. 2016, doi: 10.1147/JRD.2015.2496822.

Kusiak, A., Zheng, H., & Song, Z. (2009). On-line monitoring of power curves. Renewable Energy, 34(6), 1487–1493. doi:10.1016/j.renene.2008.10.022

Lira, A., et al. "Uncertainties in the estimate of wind energy production." Proceedings of the Energy Economics Iberian Conference, Lisbon, Portugal. 2016.

Makris, D., Smart Hybrid Energy Systems in Greek islands, Master's Thesis, University of Piraeus, 2021. (In Greek)

Maurizio FACCIO, Mauro GAMBERI, Marco BORTOLINI, Mojtaba NEDAEI. State-of-art review of the optimization methods to design the configuration of hybrid renewable energy systems (HRESs). Front. Energy, 2018, 12(4): 591–622 https://doi.org/10.1007/s11708-018-0567-x

Pagnini, L. C., Burlando, M., & Repetto, M. P. (2015). Experimental power curve of small-size wind turbines in turbulent urban environment. Applied Energy, 154, 112–121. doi:10.1016/j.apenergy.2015.04.117

Papavasiliou, A., Oren, S. S., & Aravena, I. (2015). Stochastic Modeling of Multi-area Wind Power Production. 2015 48th Hawaii International Conference on System Sciences. doi:10.1109/hicss.2015.315

Per capita consumption - Hannah Ritchie, Max Roser and Pablo Rosado (2022) - "Energy". Published online at OurWorldInData.org. Retrieved from: 'https://ourworldindata.org/energy' [Online Resource]

Petrović, V., & Bottasso, C. L. (2014). Wind turbine optimal control during storms. Journal of Physics: Conference Series, 524, 012052. doi:10.1088/1742-6596/524/1/012052

R. Palma-Behnke, F. Valencia, J. Vega-Herrera and O. Núñez-Mata, "Synthetic Time Series Generation Model for Analysis of Power System Operation and Expansion with High Renewable Energy Penetration," in Journal of Modern Power Systems and Clean Energy, vol. 9, no. 4, pp. 849-858, July 2021, doi: 10.35833/MPCE.2020.000747.

Rezamand, M., Carriveau, R., Ting, D. S.-K., Davison, M., & Davis, J. J. (2019). Aggregate reliability analysis of wind turbine generators. IET Renewable Power Generation. doi:10.1049/iet-rpg.2018.5909

Ruisheng Li, Bingxin Wu, Xianwei Li, Fengquan Zhou and Yanbin Li, "Design of wind-solar and pumped-storage hybrid power supply system," 2010 3rd International Conference on Computer Science and Information Technology, 2010, pp. 402-405, doi: 10.1109/ICCSIT.2010.5564087.

Sakki G-K, Tsoukalas I, Efstratiadis A. A reverse engineering approach across small hydropower plants: a hidden treasure of hydrological data? Hydrol Sci J 2022;67:94–106. https://doi.org/10.1080/02626667.2021.2000992.

Shafiqur Rehman, Luai M. Al-Hadhrami, Md. Mahbub Alam, Pumped hydro energy storage system: A technological review, Renewable and Sustainable Energy Reviews, Volume 44, 2015, Pages 586-598, ISSN 1364-0321, https://doi.org/10.1016/j.rser.2014.12.040.

Sklar A. Random variables, joint distribution functions, and copulas. Kybernetika 1973;9:449–460.

Technology Innovation for the Local Scale, Optimum Integration of Battery Energy Storage, a Horizon 2020 Innovation action (IA) project (February 2015 – January 2019). doi:10.3030/646529

Tsoukalas, I., Kossieris, P., & Makropoulos, C. (2020). Simulation of Non-Gaussian Correlated Random Variables, Stochastic Processes and Random Fields: Introducing the anySim R-Package for Environmental Applications and Beyond. Water, 12(6), 1645. doi:10.3390/w12061645

Tsoukalas, I., Kossieris, P., 2019. anySim: Stochastic simulation of processes with any marginal distribution and correlation structure. R package.

Vasel-Be-Hagh, A., & Archer, C. L. (2017). Wind farm hub height optimization. Applied Energy, 195, 905–921. doi:10.1016/j.apenergy.2017.03.089

Villanueva, D., & Feijóo, A. (2018). Comparison of logistic functions for modeling wind turbine power curves. Electric Power Systems Research, 155, 281–288. doi:10.1016/j.epsr.2017.10.028

Yan, J., Zhang, H., Liu, Y., Han, S., & Li, L. (2019). Uncertainty estimation for wind energy conversion by probabilistic wind turbine power curve modelling. Applied Energy, 239, 1356–1370. doi:10.1016/j.apenergy.2019.01.180

Yoon, S. H., & Oh, J. O. (2015). Prediction of long term performance for GRP pipes under sustained internal pressure. Composite Structures, 134, 185–189. doi:10.1016/j.compstruct.2015.08.075

Zafeiratou, Eleni & Spataru, Catalina. (2019). Long Term analysis of submarine transmission grid extensions between the Greek islands and the mainland. 1-6. 10.1109/SEST.2019.8849006.

Zhou, J., Erdem, E., Li, G., & Shi, J. (2010). Comprehensive evaluation of wind speed distribution models: A case study for North Dakota sites. Energy Conversion and Management, 51(7), 1449–1458. doi:10.1016/j.enconman.2010.01.020

Zisos, Athanasios, et al. Towards energy autonomy of small Mediterranean islands: Challenges, perspectives and solutions. No. EGU22-5468. Copernicus Meetings, 2022.